

# A natural variation-based screen in mouse cells reveals USF2 as a regulator of the DNA damage response and cellular senescence

Taekyu Kang,<sup>1,2</sup> Emily C. Moore,<sup>3</sup> Emily E.K. Kopania,<sup>3</sup> Christina D. King,<sup>1</sup> Birgit Schilling,<sup>1</sup> Judith Campisi,<sup>1</sup> Jeffrey M. Good,<sup>3</sup> Rachel B. Brem <sup>1,2,\*</sup>

<sup>1</sup>Buck Institute for Research on Aging, Novato, CA 94945, USA

<sup>2</sup>Department of Plant and Microbial Biology, University of California, Berkeley, CA 94720, USA

<sup>3</sup>Division of Biological Sciences, University of Montana, Missoula, MT 59812, USA

\*Corresponding author: Department of Plant and Microbial Biology, UC Berkeley, Berkeley, CA 94720, USA. Email: rbrem@berkeley.edu

## Abstract

Cellular senescence is a program of cell cycle arrest, apoptosis resistance, and cytokine release induced by stress exposure in metazoan cells. Landmark studies in laboratory mice have characterized a number of master senescence regulators, including p16<sup>INK4a</sup>, p21, NF- $\kappa$ B, p53, and C/EBP $\beta$ . To discover other molecular players in senescence, we developed a screening approach to harness the evolutionary divergence between mouse species. We found that primary cells from the Mediterranean mouse *Mus spretus*, when treated with DNA damage to induce senescence, produced less cytokine and had less-active lysosomes than cells from laboratory *Mus musculus*. We used allele-specific expression profiling to catalog senescence-dependent *cis*-regulatory variation between the species at thousands of genes. We then tested for correlation between these expression changes and interspecies sequence variants in the binding sites of transcription factors. Among the emergent candidate senescence regulators, we chose a little-studied cell cycle factor, upstream stimulatory factor 2 (USF2), for molecular validation. In acute irradiation experiments, cells lacking USF2 had compromised DNA damage repair and response. Longer-term senescent cultures without USF2 mounted an exaggerated senescence regulatory program—shutting down cell cycle and DNA repair pathways, and turning up cytokine expression, more avidly than wild-type. We interpret these findings under a model of pro-repair, anti-senescence regulatory function by USF2. Our study affords new insights into the mechanisms by which cells commit to senescence, and serves as a validated proof of concept for natural variation-based regulator screens.

**Keywords:** natural variation, novel screen, USF2, DNA damage, cellular senescence

## Introduction

Metazoan cells of many types, upon exposure to stress, can enter a senescence program, in which they stop dividing, become refractory to apoptosis, and release soluble inflammation and tissue remodeling factors termed the senescence-associated secretory phenotype (SASP) (Hayflick 1965; Campisi 2005; Campisi and d'Adda di Fagagna 2007; Coppé et al. 2008). The resulting acute immune response can clear debris, promote wound healing, and/or suppress tumorigenesis (Baker et al. 2011; Demaria et al. 2014; Paramos-de-Carvalho et al. 2021; Wan et al. 2021). However, during aging, senescent cells can remain long past any initial triggering event, resulting in chronic inflammation that damages the surrounding tissue (Krtolica et al. 2001; Parrinello et al. 2005; Davalos et al. 2010; Olivieri et al. 2018; Wan et al. 2021). Landmark studies have revealed the benefits of eliminating senescent cells to treat age-related pathologies and boost median lifespan (Baker et al. 2011; Demaria et al. 2014; Kang 2019; Kim and Kim 2019).

Establishment of the senescent state and the activity of senescent cells hinges in large part on gene regulatory events. Finding molecular players that control this process is an active area of

research. Now-classic work has implicated p16<sup>INK4a</sup> and p21 in the repression of pro-cell cycle genes and promotion of growth arrest (Campisi 2013) after DNA damage, and NF- $\kappa$ B, p53, and C/EBP $\beta$  as regulators of the SASP (Salotti and Johnson 2019). However, given the complexity of the senescence program, many more regulators likely remain to be identified. Indeed, bioinformatic approaches have identified dozens of other transcription factor candidates in senescence (Xie et al. 2014; Wang et al. 2016; Han et al. 2018; Brückmann et al. 2019; Martínez-Zamudio et al. 2020; Tyler et al. 2021; Zhang et al. 2021; Chan et al. 2022), many of which remain unvalidated (but see (Xie et al. 2014; Wang et al. 2016; Han et al. 2018; Martínez-Zamudio et al. 2020) for recent discoveries of the roles of DLX2, FOXO3 and AP-1).

We set out to develop a novel approach to survey transcription factors that play a role in cellular senescence, with the potential for increased specificity relative to traditional genomic screens. Our strategy took advantage of the natural genetic variation in senescence gene expression, and transcription factor binding sites, across mouse species. Among the top hits from this analysis, we chose the under-studied factor upstream stimulatory factor 2

Received: January 23, 2023. Accepted: April 06, 2023

© The Author(s) 2023. Published by Oxford University Press on behalf of The Genetics Society of America.

This is an Open Access article distributed under the terms of the Creative Commons Attribution License (<https://creativecommons.org/licenses/by/4.0/>), which permits unrestricted reuse, distribution, and reproduction in any medium, provided the original work is properly cited.

(USF2) for validation experiments, focusing on gene regulation and cellular phenotypes during senescence induction and maintenance.

## Methods

### Primary cell extraction and culture

Wild-derived lines of *Mus musculus* (PWK/Ph), *Mus spretus* (STF/Pas), and their interspecies F1 hybrids (*M. musculus* × *M. spretus*), were maintained in standard conditions under Montana Institutional Animal Care and Use Committee protocol number 062-1JGDBS-120418. For each genotype, five tails from two males and three females aged 3–5 months were collected into chilled Dulbecco's Modified Eagle Medium (DMEM) and shipped to the Buck Institute/UC Berkeley for further processing. *Mus domesticus* TUCA, from Tucson, Arizona, in their 40th generation of sib-sib mating, and MANB, from Manaus, Brazil, in their 25th generation of sib-sib mating, were maintained in standard conditions under UC Berkeley Institutional Animal Care and Use Committee protocol number AUP-2016-03-8548-2. For each genotype, two tails from female mice less than 10 weeks old were collected as above. No blinding was required for tail collection. Primary tail fibroblasts were extracted from the cuttings essentially as described (Khan and Gasser 2016); details are provided in Supplemental Methods. For experiments in wild-type *M. musculus*, *M. spretus*, *M. domesticus*, and F1 hybrid cells, we considered the culture from each individual animal to represent one biological replicate of the respective genotype.

### Irradiation treatment

To treat a given cell culture replicate with ionizing radiation (Campisi and d'Adda di Fagagna 2007; Zhao and Darzynkiewicz 2013; Casella et al. 2019) for a cell-biological assay or omics profiling, we proceeded as follows. The day before irradiation, cells were seeded at 60–70% confluency and incubated in a 37°C humidified incubator at 3% O<sub>2</sub> and 10% CO<sub>2</sub> overnight in complete medium. The next day, a subset of cells was collected and used as input into the respective experiment as the unirradiated control. The remainder of the culture was transferred into an X-RAD 320 X-Ray Biological Irradiator and treated with 15 Gy of X-ray irradiation. Cultures were then placed back into the 37°C humidified incubator at 3% O<sub>2</sub> and 10% CO<sub>2</sub> until sampling at 6 hours for marker assays and RNA-seq focused on acute DNA damage response, or 7, 10, or 20 days for marker assays and RNA-seq and proteomics focused on senescence (in which case the medium was replaced 6–8 hours after irradiation, then every 48 hours for the remainder of the experiment), as detailed below. For procedures used in cell proliferation and DNA damage assays, see Supplemental Methods.

### Senescence marker assays

For a given replicate culture after irradiation and incubation (see above), senescence-associated β-galactosidase (SABG) activity was measured using the BioVision Inc. Senescence Detection Kit (cat. #K320): cells were fixed, permeabilized, and incubated with the staining solution containing X-gal overnight. Multiple images were taken the following day using a brightfield microscope, and the image names were randomized before the proportion of β-galactosidase-positive cells was counted manually to remove potential sources of bias. Cultures were considered to be senescent if they showed less than 10% EdU incorporation (see below) and over 90% β-galactosidase-positive cells. In the species comparison of Fig. 1, we subjected two technical replicate cultures

of each of three biological replicates per purebred species to irradiation (see above) followed by β-galactosidase assays at the indicated timepoints. In Fig. 6c, we carried out irradiation and β-galactosidase assays as above at Day 7 after irradiation for two technical replicates from each of two biological replicates of *M. musculus* cells infected with lentivirus harboring the scrambled control and two of each *Usf2* knockdown (see below). In Supplementary Fig. 1, data from each purebred cell lines were collected on Day 10 following irradiation. In Supplementary Fig. 4, data for purebreds were from Fig. 2 at Day 7; separately, for the interspecies F1 hybrid, we carried out irradiation and β-galactosidase assays as above for two technical replicates from one biological replicate.

### RNA collection and sequencing

For a given replicate culture of a given genotype, either before irradiation or 6 hours, 10 days, or 20 days after irradiation (see above), cells were treated with TRIzol and RNA was extracted using chloroform and ethanol precipitation. The RNA was then further purified using the Qiagen RNeasy Kit (cat. #74004) for DNase treatment and column cleanup. The purity of the extracted RNA was verified using a NanoDrop ND-1000 Spectrophotometer; all samples had 260/280 and 260/230 ratios greater than 2.0. Purified RNA in distilled RNase/DNase-free water was snap-frozen using dry ice and stored at –80°C. Samples were then either transferred to the QB3 Genomics core at University of California, Berkeley, for library prep and sequencing on 150PE NovaSeq S4 or shipped to Novogene Co. (Sacramento, CA) for the same. Both facilities provided 25 million paired end reads per sample. For expression profiles of purebred cells and *M. musculus* × *M. spretus* F1 hybrid cells, we subjected three biological replicates of a given genotype to irradiation (see above) followed by RNA-seq at the indicated timepoints. To assess transcriptional impacts of *Usf2* knockdown, we carried out irradiation and RNA isolation as above for two biological replicates of *M. musculus* cells infected with lentivirus harboring the scrambled control and two of each *Usf2* knockdown (see below).

### Pseudogenome and VCF generation

As publicly available annotations for *M. musculus* and *M. spretus* are in the context of their reference genomes (GRCm38.96 and SPRET\_Eij\_v1.96, respectively), custom pseudogenomes for strains PWK and STF were generated and used for this study. For the PWK pseudogenome, variant calls between PWK and the reference genome in the form of a variant call file (VCF) were downloaded from the Sanger Mouse Genomes Project database (<https://www.sanger.ac.uk/data/mouse-genomes-project/>). A pseudogenome using the VCF and the GRCm38.96 reference genome was created using bcftools v1.9 (Danecek et al. 2021). To generate shotgun sequence data for the STF pseudogenome, DNA was extracted from *M. spretus* liver tissue using Qiagen DNeasy spin columns (cat. #69506). The sample was sheared via sonication (Covaris E220), and prepared using the New England Biolabs NEBNext Ultra DNA Library kit (cat. #E7370L). The final library was sequenced on a single lane of 150-bp PE Illumina HiSeq X at Novogene, Inc. The latter reads were aligned to the SPRET\_Eij\_v1.96 reference genome using bowtie v2.2.3 (Langmead and Salzberg 2012), and a VCF was generated using bcftools mpileup and filtered for quality, depth, and SNPs using vcftools (Li et al. 2009; Li 2011). The VCF was then used with the reference genome to create a STF pseudogenome using bcftools. The pseudogenomes were verified by identifying a number of called variants by hand. A VCF of variants between the STF and PWK

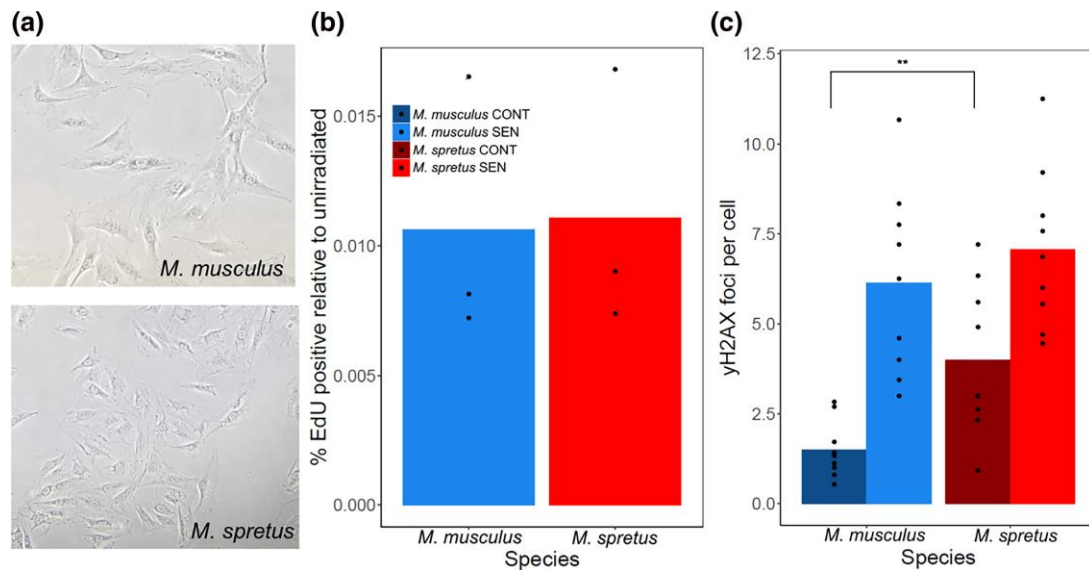


**Fig. 1.** Phenotypes of senescence in cells from *M. musculus* and *M. spretus* mice. a) Representative images of senescent primary fibroblasts from *M. musculus* and *M. spretus* 7 days after irradiation exhibiting a flattened and enlarged morphology. b) Each column reports the average percentage of cells with EdU incorporation 7 days after IR treatment (SEN) set relative to the same in unirradiated controls (CONT) for each species reported in (A). For a given column, points report biological and technical replicates (*M. musculus*  $n = 3$ , *M. spretus*  $n = 3$ ). c) Each column reports the average number of  $\gamma$ -H2AX foci per cell for cells of the indicated genotype and treatment. For a given column, points represent biological and technical replicates (*M. musculus*  $n = 9$ , *spretus*  $n = 9$ ). \*\*,  $P < 0.01$ , one-tailed Wilcoxon test comparing species.

pseudogenomes was generated as above aligning the STF whole genome sequencing reads to the PWK pseudogenome.

### RNA-seq processing

In transcriptional profiles of *M. musculus*  $\times$  *M. spretus* F1 hybrid cells, sequencing reads from a given replicate were aligned to a concatenated PWK/STF pseudogenome using tophat v2.1.1 (Kim, Pertea, et al. 2013) allowing for zero mismatches to ensure allele specific mapping. Alignments were then filtered for uniquely mapped reads using samtools v1.3.1, and gene counts were generated using HTSeq v0.11.2 (Putri et al. 2022) and genome annotations (GRCm38.96, SPRET\_EiJ\_v1.96) for both species from Ensembl. Counts were then converted to transcripts per million (TPM) using custom R scripts, and genes were filtered for those showing counts in more than half the samples sequenced.

In transcriptional profiles of purebred *M. musculus* wild-type cells and *M. musculus* cells infected with lentiviruses harboring shRNAs, RNA-seq processing was as above but mapping was to the PWK pseudogenome only; for profiles of purebred *M. spretus* wild-type cells, mapping was to the STF pseudogenome only.

Data for the average TPM across biological replicates for purebred parents and interspecific F1 hybrid are reported in Supplementary Table 1. Average TPM across biological replicates for shRNA-treated *M. musculus* cells are reported in Supplementary Table 6.

### Gene Ontology enrichment analysis of RNA-seq data

For the comparison of transcriptional profiles of *M. musculus* and *M. spretus* purebred cells, for each gene in turn, we tabulated the average TPM count from each species across replicates, and then took the  $\log_2$  of the ratio of these averages,  $r_{\text{sen, true}}$ . We downloaded Gene Ontology annotations from the AmiGO 2 (Ashburner et al. 2000; Gene Ontology Consortium 2021) database and filtered for those with supporting biological data. For each term, we summed the  $r_{\text{sen, true}}$  values across all genes of the term, yielding

$s_{\text{sen, true}}$ . To assess the enrichment for high or low values of this sum, we first took the absolute value,  $|s_{\text{sen, true}}|$ . We then sampled, from the total set of genes with expression data, a random set of the same number as that in the true data for the term; we calculated the species difference  $r_{\text{sen, rand}}$  for each such gene and the absolute value of the sum over them all,  $|s_{\text{sen, rand}}|$ . We used as a P-value the proportion of 10,000 resampled data sets in which  $|s_{\text{sen, true}}| > |s_{\text{sen, rand}}|$ .

For analysis of the impact of *Usp2* knockdown on expression before or 6 hours, 10 days, or 20 days after irradiation (see below), Gene Ontology enrichment tests were as above except that we took the ratio, for a given gene, between the average expression in purebred *M. musculus* (PWK) cells infected with lentivirus harboring scrambled shRNA and the analogous quantity across both *Usp2*-targeting shRNA treatments.

### Proteomic analysis of secreted proteins

For a given replicate culture, either before irradiation or 10 days after irradiation (see above), cells were washed three times with PBS and incubated with serum and phenol red free DMEM containing 1% pen-strep for 24 hours. The following day, the conditioned medium was collected and passed through a 0.45- $\mu$ m filter to remove cellular debris. The conditioned medium was placed in a  $-80^\circ\text{C}$  freezer for storage before use as input into proteomic profiling (see below). For proteomic profiles of purebred cells, we carried out this procedure for three technical replicate cultures of one biological replicate per species.

Sample processing for quantitative proteomic analysis via mass spectrometry was performed as in Neri et al. (2021); details are provided in Supplemental Methods.

### Transcriptomic screen for senescence regulators

To associate expression variation in genes with sequence variation in their upstream binding sites for a given transcription factor, we proceeded as follows. From RNA-seq profiling of *M. musculus*  $\times$  *M. spretus* F1 hybrid cells (see above), we used the

TPM counts for each parent species' allele from each replicate profile from control and senescent conditions as input into a two-factor ANOVA. A given gene was categorized as exhibiting senescence-associated differential allele-specific expression if the interaction F statistic value from this ANOVA was among the top 25% of all genes tested. Separately, we used compiled data from chromatin immunoprecipitation via high-throughput sequencing from the Gene Transcription Regulation Database (Yevshin et al. 2019) to identify all experimentally determined transcription factor (TF) binding sites located within a 5-kb window upstream of the transcriptional start site for each gene in turn in the *M. musculus* genome; we refer to the downstream gene of each such binding location as the target of the TF. This calculation used *M. musculus* gene start sites from the Ensembl GRCm38.96 GFF. Next, for each binding site, we used the VCF between PWK and STF pseudogenomes (see above) to identify single nucleotide variants between PWK and STF in the binding site locus. Now, for all the target genes of a given TF, we categorized them as having sequence variants or not in the respective binding site, and exhibiting senescence-associated differential allele-specific expression. We eliminated from further consideration any TF with fewer than 250 target genes in each of the four categories. For all remaining TFs, the  $2 \times 2$  contingency table was used as input into a Fisher's exact test with Benjamini-Hochberg multiple testing correction.

### Usf2 shRNA vector design, construction, and application

Usf2 knockdown shRNA sequences were obtained from the Broad Institute Genetic Perturbation Portal (<https://portals.broadinstitute.org/gpp/public/>). Two shRNA sequences for Usf2 (CCGGGCAAGACAGGAGCAAGTAAAGCTCGAGCTTTACTTGCTCCTGTCTTGTCTTTTTTGAAT; CCGGACAAGGAGACATAATGCATTCTCGAG-AAATGCATTATGTCTCCTTGTCTTTTTTGAAT), and, separately, a scrambled control sequence (CCTAAGGTTAAGTCGCCCTCGCTCGAGCGAGGGCGACTTAACCTTAGG, Addgene cat. #1864) were each cloned into pLKO.1 puro lentiviral vectors (Addgene cat. #8453). Lentiviral particles containing each of the shRNA constructs were generated by calcium phosphate co-transfection of HEK 293T cells with the shRNA pLKO.1 puro vectors and separate pMDLg/pRRE packaging and pCMV-VSV-G envelope plasmids generously provided by Dr. Marius Walter of the Verdin Lab at the Buck Institute. The number of viral particles generated was determined using the Origene One-Wash Lentivirus Titer Kit, p24 ELISA (cat. #TR30038). These particles were used to infect two biological replicates of purebred *M. musculus* (PWK) primary tail fibroblasts at a multiplicity of infection of 5 with 4  $\mu\text{g}/\text{mL}$  of polybrene, and infected cells were selected by incubating with 2- $\mu\text{g}/\text{mL}$  puromycin for 10 days, changing media and antibiotic every other day. Knockdown of Usf2 was determined by qPCR, using Usf2 qPCR primer sequences chosen through NCBI Primer Blast, filtering for those spanning an exon-exon junction. The primer pair with the same efficiency (calculated as  $10^{(-1/\text{slope})}$  when plotting log concentration of template cDNA vs Ct) as the internal control Actb qPCR primers was chosen: Usf2 forward 5' TTCGGCGACCACAATATCCAG 3', Usf2 reverse 5' TTCGGCGACCACAATATCCAG 3', Actb forward 5' CAACCGTGAAAAGATGACCC 3', Actb reverse 5' GTAGATGGGCACAGTGTGGG 3'. Usf2 expression was calculated using the Delta-Delta Ct method (Livak and Schmittgen 2001).

### Cell proliferation and DNA damage assays

For each of two biological replicates of purebred *M. musculus* (PWK) cells infected with lentivirus harboring the scrambled control and two of each Usf2 knockdown, either before irradiation or 6 hours after irradiation (see above), we measured cell proliferation and DNA damage response as follows.

For a given replicate, DNA synthesis was measured via 5-ethynyl-2'-deoxyuridine (EdU) incorporation assays using the Invitrogen Click-iT Edu Alexa Fluor 488 Flow Cytometry Assay Kit (cat. #C10420). Comet assays were carried out to measure levels of DNA double-stranded breaks for a given replicate culture as described (Olive and Banáth 2006).

For H2AX assays, for a given replicate, cells were fixed, permeabilized, and blocked, then incubated with 1  $\mu\text{g}/\text{mL}$  of primary antibodies specific to phosphorylated (Ser 139) H2AX (cat. #sc-517348, Santa Cruz Biotechnology) in 3% BSA overnight at 4°C. The following day, the cells were washed in PBS three times before incubating with 2  $\mu\text{g}/\text{mL}$  of Alexa 488 secondary antibodies purchased from Invitrogen (cat. #A11001) for 2 hours at room temperature. Cells were washed three times with PBS then incubated with 0.5- $\mu\text{g}/\text{mL}$  DAPI for 5 minutes at room temperature. The cells were washed once more with PBS before mounting for imaging. Multiple representative confocal images of each sample were taken using a Zeiss LSM 710 AxioObserver, and processed with ImageJ (Schneider et al. 2012).

### Multivariate ANOVA of irradiation and senescence timecourse

To identify genes whose expression changed in wild-type cells through irradiation and senescence, we used RNA-seq profiling data from purebred *M. musculus* (PWK) cells harboring a scrambled shRNA before and 6 hours, 10 days, and 20 days after irradiation (see Supplementary Table 6) as input into a multivariate ANOVA test.

### MERLIN regulatory network reconstruction

To reconstruct a regulatory network, we used RNA-seq profiling data for purebred *M. musculus* (PWK) cells harboring a scrambled shRNA or a Usf2-targeting RNA, before and 6 hours, 10 days, and 20 days after irradiation, as input into MERLIN (Roy et al. 2013) with default settings. Analysis used a catalog of murine transcription factors from the Gene Transcription Regulation Database (Yevshin et al. 2019).

## Results

### High levels of senescence markers in *M. musculus* fibroblasts relative to other mice

To study natural variation in senescence phenotypes, we made use of a classic in vitro cell model of senescence, namely primary fibroblasts from mouse tail skin treated with 15 Gy of ionizing radiation (IR) (Campisi and d'Adda di Fagagna 2007; Casella et al. 2019). We isolated primary tail fibroblasts from the PWK and STF wild-derived purebred lines of *Mus musculus musculus* (hereafter *M. musculus*) and *M. spretus*, respectively. Seven days after IR treatment, cells from both species had arrested growth and exhibited the expected flattened and enlarged morphologies of senescent cells (Fig. 1a and b). Assaying these cultures for  $\gamma$ -H2AX foci, a marker of the DNA damage response and a hallmark of long-term senescence (Rodier et al. 2009; Siddiqui et al. 2015), we found that counts were indistinguishable in primary *M. musculus* and *M. spretus* fibroblasts after irradiation, though higher in the

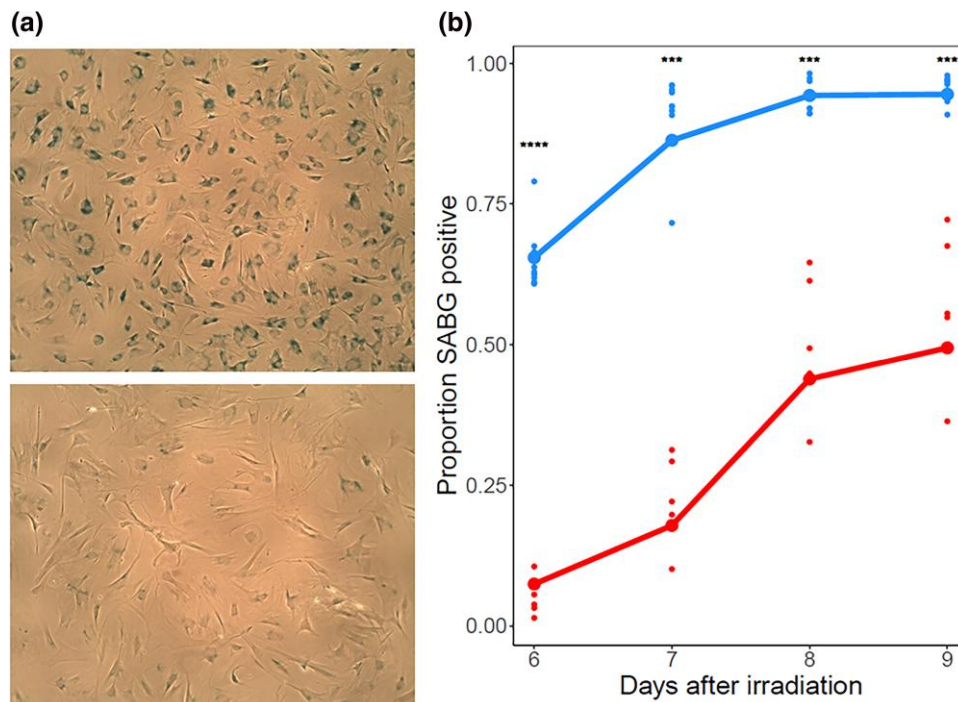


**Fig. 2.** Senescent *M. spretus* cells exhibit lower  $\beta$ -galactosidase activity. a) Representative images of senescent primary fibroblasts from *M. musculus* (above) and *M. spretus* (below) stained with the  $\beta$ -galactosidase indicator X-Gal seven days after irradiation. b) Each trace reports results from a timecourse of X-Gal staining assays of primary senescent cells of the indicated species as in (A). The y-axis reports the proportion of cells stained positive for SABG activity. In a given column, small points report biological and technical replicates and large points report their average (*M. musculus*  $n = 9$ , *M. spretus*  $n = 5$ ). \*\*\*,  $P < 0.001$ , \*\*\*\*,  $P < 0.0001$ , one-tailed Wilcoxon test comparing species.

latter in the absence of treatment (Fig. 1c). These data indicated that cells of both species had mounted the DNA damage response and entered the senescent state in our treatment and incubation regime.

To begin to compare the senescence program between cells of *M. musculus* and *M. spretus*, we assayed primary fibroblasts from each species for SABG, which reports lysosomal hyperactivity during senescence and has served as a classic marker of senescence (Dimri et al. 1995). After irradiation, we detected robust signal in this assay from cells of both species, as expected; however, the proportion of SABG-positive cells in *M. spretus* fibroblast cultures was two to eight-fold lower than that of *M. musculus* cells (Fig. 2). Primary fibroblasts from *M. musculus domesticus*, a close relative of *M. musculus musculus*, exhibited an intermediate SABG staining after irradiation (Supplementary Fig. 1). We conclude that in the irradiated fibroblast culture model, genotypes from distinct species encode a range of lysosomal activity phenotypes, with the most avid in *M. musculus musculus*.

### The high-amplitude SASP of *M. musculus* fibroblasts is unique relative to *M. spretus*

In *M. musculus* cells, the massive lysosomal changes seen after irradiation likely result from overload of the proteostasis system during SASP production (Brunk and Terman 2002; Pluquet et al. 2015; Park et al. 2018). Given that we had observed weaker effects of irradiation on lysosomal activity in fibroblasts from non-*M. musculus* species (Supplementary Fig. 1), we hypothesized that the latter would likewise exhibit a dampened-SASP phenotype. To test this, we focused on *M. musculus* and *M. spretus* as representatives of the extremes of the phylogeny. We profiled bulk RNA levels in irradiated and control primary fibroblast cultures from each species (Supplementary Table 1). In the resulting profiles,

we inspected genes of the SASP immune-stimulatory program (Coppé et al. 2008), and found that this gene cohort was induced more highly in *M. musculus* cells than in those of *M. spretus* after irradiation (Fig. 3a). Likewise, in an unbiased search of Gene Ontology terms, we identified several suites of immune response and NF- $\kappa$ B signaling genes that were enriched for senescence-specific differential expression between the cultures (Fig. 3b and Supplementary Tables 2 and 3). In each case, the gene groups were more strongly induced during senescence in *M. musculus* cells than in *M. spretus* cultures; among members of the latter, we noted *Cxcl1* (Kim et al. 2018), *Il6* (Coppé, Patil, et al. 2010), *Ccl2*, 7, and 8 (Coppé, Desprez, et al. 2010), *Mmp13* (Levi et al. 2020), and other reported SASP genes (Supplementary Fig. 2). These data make clear that, at the level of mRNA expression, the senescence regulatory program differs markedly between fibroblasts of our focal species.

We hypothesized that much of the mRNA expression divergence between *M. musculus* and *M. spretus* cells during senescence would result in differential protein abundance. In pursuing this notion, we focused on proteins secreted into the medium by senescent cells, owing to the physiological importance of the SASP (Coppé, Desprez, et al. 2010). We collected conditioned media from senescent and control cultures of primary fibroblasts of each genotype, and we used it as input into unbiased mass spectrometry to quantify protein abundance (Supplementary Table 4). Focusing on proteins with a significant senescence-specific divergence in secretion between cells of the two species in this data source, we found higher levels overall in the medium of irradiated *M. musculus* cells relative to that of *M. spretus* (Fig. 3c). This trend was borne out for a broad representation of SASP factors, including CCL chemokines, matrix metalloproteases, and serpins (Supplementary Fig. 3). Together, our omics profiles reveal

pervasive, quantitative differences in SASP levels between *M. spretus* fibroblasts and those of *M. musculus*, with higher mRNA expression and protein secretion in the latter.

### A genomic screen for senescence transcription factors using cis-regulatory sequence variations

Having established divergence between *M. musculus* and *M. spretus* primary fibroblasts in senescence mRNA and protein secretion (Fig. 3), we reasoned that such differences could be harnessed in an *in silico* screen for senescence regulators. We designed an analysis focused on gene regulation—in particular, on variation between the species at the binding sites of transcription factors (Fig. 4a). We expected that, at some genes, cis-regulatory elements encoded in the *M. musculus* genome would drive expression during senescence differently than those in the *M. spretus* genome. We reasoned that if cis-acting variation effects were enriched among the loci bound by a given transcription factor across the genome, the signal could be interpreted as a signpost for the factor's activity during senescence (Fig. 4a). In this way, all cis-regulatory variants between the species that manifested in cultured primary fibroblasts, whether of large or small effect size, and regardless of their potential for phenotypic impact, could contribute to the search for transcription factors relevant for senescence.

As a resource for this approach, we mated PWK *M. musculus* and STF *M. spretus* to yield F1 hybrid animals, from which we derived primary tail fibroblasts for culture and irradiation. These cells, when irradiated, exhibited a flattened morphology reflecting entry into senescence; SABG activity was of a magnitude between those of purebred *M. musculus* and *M. spretus* fibroblasts upon irradiation (Supplementary Fig. 4). We subjected senescent and control F1 hybrid fibroblasts to RNA-seq profiling, and we used the results to quantify levels of transcripts derived from the *M. musculus* and *M. spretus* alleles of each gene in each condition (Supplementary Table 1). At a given gene, any difference between allele-specific expression in an F1 hybrid can be attributed to variants inherited from the parent species that perturb gene regulation in *cis* at the locus, because *trans*-acting factors impinge to the same extent on both alleles (Sun and Hu 2013). Analyzing the response to senescence induction for a given gene, we found that the allele-specific expression difference between the alleles in the F1 hybrid was a partial predictor of the expression divergence between the *M. musculus* and *M. spretus* purebreds, in our primary cell system (Supplementary Fig. 5). The latter trend reflects the joint contributions of *cis*- and *trans*-acting variants to total expression divergence between the species, as expected (Wittkopp et al. 2004). Separately, to survey overall regulatory programs in F1 hybrid primary fibroblasts, we formulated the expression level of a given gene in a given condition as the sum of the measured levels of the *M. musculus* and *M. spretus* alleles. In this analysis, focusing on SASP genes as we had done for the purebreds (Fig. 3a), we found that the expression program of senescent F1 hybrid cells was, for most components, intermediate between the low levels seen in *M. spretus* cells and the high levels in *M. musculus* (Supplementary Fig. 6). These data indicate that *M. musculus* × *M. spretus* F1 hybrid fibroblasts do not exhibit heterosis with respect to senescence-associated genes, and do manifest extensive, senescence-dependent cis-regulatory variation.

We next used the expression measurements from *M. musculus* × *M. spretus* F1 hybrid fibroblasts as input into our *in silico* screen to identify senescence-dependent transcription factor activity. For a given transcription factor, we collated binding sites detected by chromatin immunoprecipitation upstream of genes across a panel of tissues (Yevshin et al. 2019). At each site, we

tabulated the presence or absence of DNA sequence variants in the respective genomes of *M. musculus* and *M. spretus*. We then tested whether, across the genome, genes with these binding site variants were enriched for senescence-associated expression differences between the two alleles in the F1 hybrid. This test had the capacity for high power to detect even subtle contributions from transcription factors if they had deep binding-site coverage in the input data; five factors attained genome-wide significance (Fig. 4b and Supplementary Table 5). Among them, PBX1 (Wang et al. 2021) and CREBBP (Bandyopadhyay et al. 2002; Yang et al. 2021) had been implicated in cellular senescence in the previous literature, providing a first line of evidence for the strength of our approach to identify signatures of condition-dependent transcription factor function. The top-scoring transcription factor in our screen, a basic-helix-loop-helix leucine-zipper protein called USF2, had not been experimentally characterized in stress response or senescence. However, classic studies had established USF2 as a regulator of the cell cycle and tumor suppression (Aperlo et al. 1996; Qyang et al. 1999; Pawar et al. 2004; Chen et al. 2006; Qi et al. 2006; Qi et al. 2014). More recently, USF2 was shown to control cytokine release in immune cells (Hu et al. 2020). Considering these known functions, and bioinformatic analyses suggesting a link between USF2 and senescence programs (Allen et al. 2005; Martínez-Zamudio et al. 2020), we chose USF2 for in-depth validation. In detailed genomic tests, single variants between *M. musculus* and *M. spretus* at USF2 binding sites drove most of the relationship with allele-specific expression in hybrid senescent cells (Fig. 4c). These variants were over-represented at positions central to, and slightly downstream of, experimentally determined peaks for USF2 (Fig. 4d), highlighting the likely importance of the latter region in USF2's mechanisms of binding and regulation.

### USF2 modulates cell proliferation and the acute DNA damage response

Our question at this point was whether and how USF2 regulated senescence programs. As such, we shifted our focus from natural genetic variation to controlled, laboratory-induced genetic perturbations in a single genetic background. We designed two short hairpin RNAs (shRNAs) targeting *Usf2*, each in a lentiviral vector under the U6 promoter. Expression measurements upon transformation of PWK *M. musculus* primary tail fibroblasts confirmed 2.5 and 3-fold knockdown of *Usf2* expression, respectively, from these shRNAs (Supplementary Fig. 7). In these otherwise untreated cells subject to knockdown, uptake of the nucleotide analog EdU, a marker of DNA synthesis, was reduced by 40% (Supplementary Fig. 8), consistent with studies of USF2 in growth of resting cells in other tissues and contexts (Aperlo et al. 1996; Qyang et al. 1999; Pawar et al. 2004; Allen et al. 2005; Chen et al. 2006; Qi et al. 2006; Zhao and Darzynkiewicz 2013; Qi et al. 2014).

We now set out to use our knockdown approach to define the role of USF2 in the acute DNA damage response and senescence. For this purpose, we infected cells with *Usf2* shRNAs, cultured them under standard conditions, and then subjected them to irradiation. DNA damage signaling, an inducer of cellular senescence (Campisi 2005; Campisi and d'Adda di Fagagna 2007), drops sharply in intensity within 8 hours and then more gradually over several days after irradiation (Redon et al. 2009), culminating in a lower persistent signal (Bakkenist et al. 2004; Chen and Ozanne 2006; Fumagalli et al. 2014; Siddiqui et al. 2015). We first focused on the early phase of this process (6 hours after irradiation) in cultures of primary fibroblasts expressing *Usf2* shRNAs or scrambled shRNA controls (Fig. 5a). Transcriptional profiling

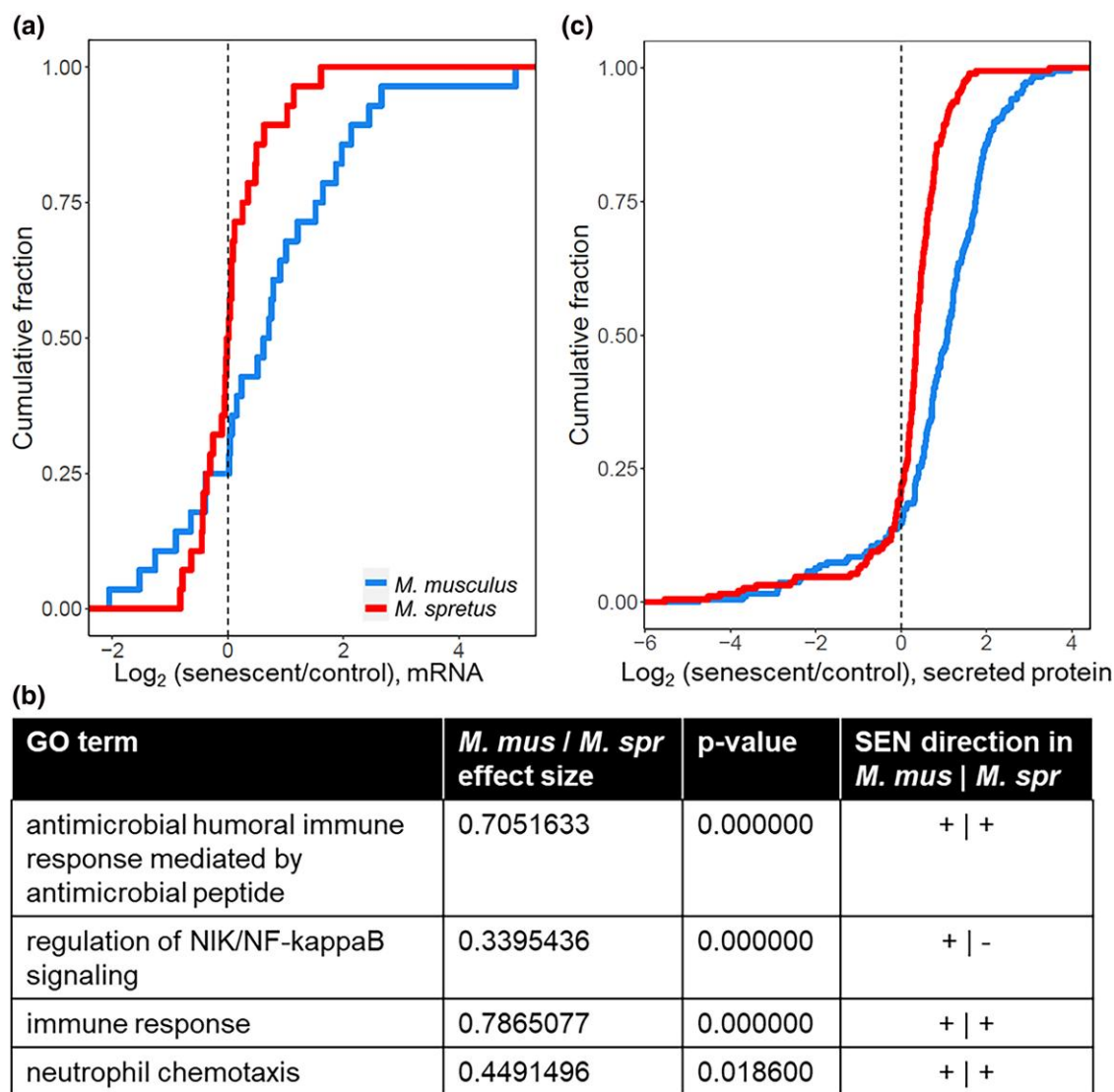


**Fig. 3.** SASP is detected at higher levels in *M. musculus* cells. a) Each trace reports a cumulative distribution of the change, in senescent primary fibroblasts of the indicated species, in mRNA levels of genes of the senescence-associated secretory phenotype with senescence (Coppé et al. 2008). The y-axis reports the proportion of genes with the expression change on the x-axis, with the latter taken as an average across replicates. b) Each row shows results from a test of the genes of the indicated Gene Ontology term for enrichment of expression change between the species during senescence, with P-values from a resampling-based test, corrected for multiple testing. c) Annotations are as in (A) except that measurements were of secreted peptides, and results from a curated list of known SASP factors are shown (Coppé et al. 2008; Basisty et al. 2020).

followed by Gene Ontology analyses identified gene groups enriched for expression changes dependent on condition and USF2 (Fig. 5b and Supplementary Tables 6 and 7). Most salient was a trend of pervasive repression transcriptome-wide 6 hours after irradiation, which was detected in control cells as expected (Venkata Narayanan et al. 2017; Silva and Ideker 2019), and was blunted in cells with *Usf2* knocked down. The latter effect was particularly enriched in the transcriptional machinery, repressors of apoptosis, and several cell proliferation regulators (Fig. 5b–d and Supplementary Fig. 9). DNA repair genes, a likely target for changes upon irradiation, are regulated primarily at the post-transcriptional level (Nickoloff et al. 2017; Huang and Zhou 2020), and we did not detect effects of *Usf2* knockdown on their transcripts (Supplementary Fig. 10).

We hypothesized that *Usf2* knockdown during the acute DNA damage response would also have cell-physiological effects. Assays of EdU incorporation to report on DNA synthesis showed

effects of *Usf2* knockdown after irradiation to the same degree as in resting cultures (Supplementary Fig. 7). To focus on phenotypes more proximal to DNA damage, we used the neutral comet assay (Olive and Banáth 2006) to measure DNA double-stranded breaks on a per-cell basis. In this setup, *Usf2* depletion increased comet tail moments by 50% 6 hours after irradiation, with an effect that was similar, though of smaller magnitude, in resting cell controls (Fig. 5e). Next, we tracked foci of phosphorylated histone H2AX ( $\gamma$ -H2AX) in fibroblasts as a marker of chromatin decondensation, preceding the repair of DNA double-stranded breaks (Podhorecka et al. 2010). Cells harboring *Usf2* shRNAs exhibited 30% fewer  $\gamma$ -H2AX foci than cells of the control genotype, six hours after irradiation (Fig. 5f). These data establish a role for USF2 in the response to irradiation, with knockdown of this factor compromising cells' ability to mount the classical transcriptional program under this stress, and to carry out DNA damage repair.

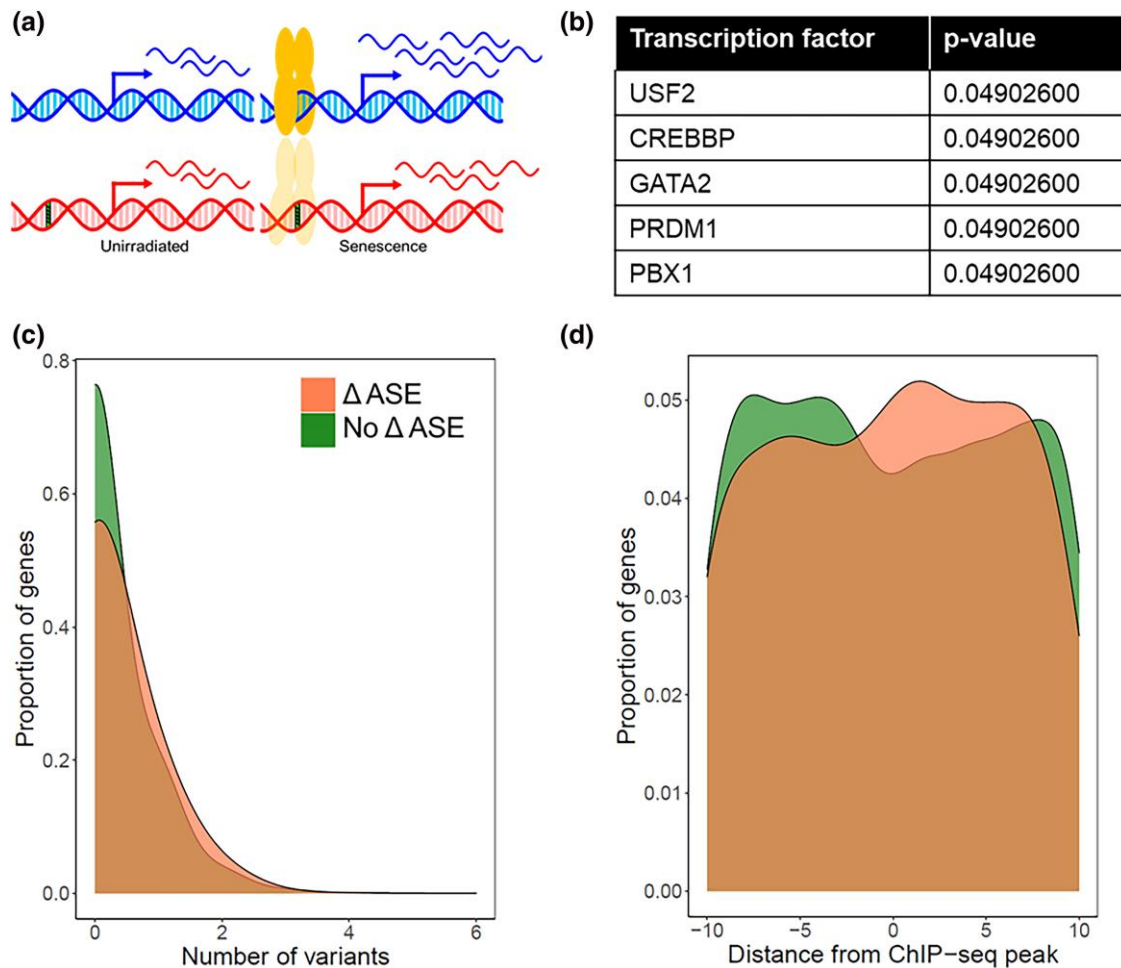


**Fig. 4.** USF2 emerges as a senescence regulator candidate from a natural variation-based transcription factor screen. a) *M. musculus* (blue) and *M. spretus* (red) alleles of a gene are expressed differently in interspecific F1 hybrid cells in a senescence-dependent manner, as a product of a sequence variant (green striped) in the binding site for a transcription factor (yellow). b) Each row reports the multiple testing-corrected *P*-value from a Fisher's Exact Test of target genes of the indicated transcription factor, quantifying association between species differences in experimentally determined binding sites (Yevshin et al. 2019) and allele-specific expression in primary cells of the *M. musculus* × *M. spretus* F1 hybrid background before and after senescence induction. Results for all tested factors are listed in Supplementary Table 5. c) Shown are the input data for the Fisher's Exact Test in (B) for USF2. For each trace, the x-axis reports the number of sequence variants between *M. musculus* and *M. spretus* in a given USF2 binding site, and the y-axis reports the proportion of all USF2 target genes bearing the number of variants on the x, as a kernel density estimate. Colors denote the presence or absence of senescence-dependent differential allele-specific expression (ΔASE). d) Data are as in (C) except that the x-axis reports the distance of the variant from the center of the USF2 binding site.

### USF2 tunes the commitment to senescence

Having knocked down *Usf2* in PWK primary fibroblasts and irradiated them to study the acute DNA damage response, we now allowed the irradiated cultures to enter senescence (Fig. 6a). We referred to this as a “knockdown-then-irradiate” experimental design (SH→SEN in Fig. 6). Growth arrest and flattened morphology were indistinguishable between these cells and controls harboring scrambled shRNAs (see Fig. 6c), indicating that wild-type levels of *Usf2* were not required at the point of irradiation to establish senescence per se. To investigate quantitative characteristics of these senescent cultures, we subjected them to expression profiling and Gene Ontology enrichment analyses (Fig. 6b and Supplementary Tables 6 and 8). Among top-scoring gene groups, the most dramatic effects were in those that dropped in expression in senescent cultures of the control genotype, which as expected (Kim, Byun, et al. 2013; Chan et al. 2022) included cell cycle and DNA repair pathways (Fig. 6b and Supplementary Table 8). Intriguingly, mRNA levels of the latter were even lower

in senescent cells that had been irradiated after *Usf2* knockdown, showing a reduction of ~20% on average (Fig. 6b). Among the genes of this cohort, some of which declined in expression by >5-fold with *Usf2* knockdown in senescence, we noted cell cycle regulators (*Ccna2*, *Cdc20*, and *Cdk1*), kinesin components (*Kif2c* and *Knl1*), the DNA polymerase *Pole*, and the DNA damage checkpoint ubiquitin ligase *Uhrf1* (Supplementary Fig. 11a). We conclude that genes of the cell cycle and DNA repair machinery are detectable at a low but non-zero expression level in wild-type senescent cells, and that these pathways are subject to further reduction when *Usf2* is limiting.

Likewise, *Usf2* knockdown before irradiation and senescence development also affected inflammation and immune-recruitment factors (Fig. 6b and Supplementary Table 8). Cells of the control genotype induced these pathways during senescence, as expected (Campisi 2005; Campisi and d'Adda di Fagnagna 2007; Coppé, Patil, et al. 2010; Olivieri et al. 2018; Santoro et al. 2018; Kale et al. 2020); in cells reaching senescence after *Usf2* knockdown, induction of inflammatory factors was amplified by ~10% on average (Fig. 6b and



Supplementary Fig. 11b). Similarly, in assays of the  $\beta$ -galactosidase senescence marker, we observed a 10% increase in cells subject to *Usf2* knockdown and senescence treatment (Fig. 6c). Together, our profiling data establish that irradiation of primary fibroblasts with reduced *Usf2* expression leads to a quantitatively perturbed, exaggerated senescent state, with reduced expression of proliferation and DNA repair pathways, and elevated pro-inflammatory gene expression and  $\beta$ -galactosidase activity.

We reasoned that the changes in senescence we had seen upon irradiation of *Usf2*-depleted cells could constitute, in part, effects from increased DNA damage in the knockdown genotype (Fig. 5). To pursue the role of USF2 in senescence more directly, we used a distinct experimental paradigm: we irradiated wild-type cells and incubated them for 10 days to allow establishment of senescence, and we then expressed shRNAs targeting *Usf2*, followed by 10 additional days of incubation (Fig. 6d). We referred to this as an “irradiate-then-knockdown” experiment (SEN→SH in Fig. 6). We first inspected control cells for this paradigm, harboring a scrambled shRNA. Here RNA-seq revealed expression changes for many genes from the resting state through irradiation and early and late senescence (Supplementary Tables 6 and 9, and Supplementary Fig. 12), attesting to the dynamics of senescence as expected (Kim, Byun, et al. 2013; Chan et al. 2022). We next carried out RNA-seq and Gene Ontology term enrichment analysis of cultures subject to *Usf2* knockdown during late senescence (Fig. 6d–g and Supplementary Tables 6 and 10), for comparison to our “knockdown-then-irradiate” strategy (Fig. 6a). On average, cell cycle and DNA repair genes, repressed in control cells during senescence, were expressed at even lower levels when *Usf2* was knocked down midway through the senescence time course; this was analogous to our findings upon early knockdown of *Usf2* (compare lavender to magenta in Fig. 6g and Supplementary Fig. 11a). Likewise, inflammatory response factors, induced during senescence in the control setting, were more highly expressed in the “irradiate-then-knockdown” approach, consistent with our findings from the early-knockdown design (compare lavender to magenta in Fig. 6f and Supplementary Fig. 11b). We noted only a handful of genes for which early *Usf2* knockdown effects were not recapitulated in our paradigm of knockdown after senescence entry (e.g. *Adamts1* and *Rarres2* in Supplementary Fig. 11b). Overall, our analyses establish USF2 as a senescence regulator at least in part independent of its role in the acute DNA damage response, such that in its absence, cells commit even more strongly to the senescent state.

## Discussion

Complex regulatory networks likely underlie many of the quantitative behaviors of senescent cells, including kinetics and dependence on cell type and inducer (Campisi 2013; Purcell et al. 2014; Casella et al. 2019; Basisty et al. 2020; Chan et al. 2022). Exactly how these nuances are encoded remains poorly understood. To date, discovery of senescence regulators has proceeded via screens of laboratory-induced gain- or loss-of-function (Wang et al. 2016; Han et al. 2018; Brückmann et al. 2019; Tyler et al. 2021), or inferences from expression and chromatin profiles (Martínez-Zamudio et al. 2020; Zhang et al. 2021; Chan et al. 2022). In this study, we pioneered the use of interspecies genetic divergence for this purpose. Our approach harnesses the correlation between interspecies variation in sequence and expression levels, as a line of evidence for senescence-specific regulatory functions by a given factor. This paradigm parallels similar tools previously used to dissect divergence in expression (Veyrieras

et al. 2008; Villarroel et al. 2021) and transcription factor binding (Heinz et al. 2013; Vierbuchen et al. 2017; Yang et al. 2022) in other contexts. Broadly speaking, these methods are not highly powered for essential determinants of a pathway under strong evolutionary constraint, which, by definition, will not vary enough among species to yield the raw observations that would go into a screening pipeline. It is likely owing to the latter effect that many previously characterized senescence regulators did not rise to high significance in our screen results. Rather, our natural variation-based approach is well-suited to identify modifiers under modest evolutionary constraint, many of which may act to confer layers of quantitative regulation onto a master regulatory pathway.

We focused our experimental validation on one such modifier, the transcription factor USF2. This factor and its family member USF1 have been well characterized for their role in cell cycle regulation and tumor suppression, with both pro- and antiproliferative roles reported across cell types (Qyang et al. 1999; Pawar et al. 2004; Allen et al. 2005; Chen et al. 2006; Qi et al. 2006; Qi et al. 2014; Hu et al. 2020). By tracing USF2’s function in proliferation and genome-wide expression in untreated cells, we extended these conclusions alongside other documented functions of USF2 in apoptosis (Sato et al. 2011) and ERK1/2 signaling (Chi et al. 2020). In an acute DNA damage setting, we discovered that USF2 is required for cells to mount DNA repair and downstream DNA damage responses. And in senescence proper, in our cell culture system, we showed that USF2 acts as a repressor, such that in its absence, the senescence program—shutoff of cell proliferation and DNA repair, and induction of cytokines—is amplified. A compelling model is thus that even long after damage exposure, cells have access to expression states along a continuum of commitment to senescence and that USF2 acts to help determine which state they occupy. If so, USF2 would take a place among a network of factors, including p53, ING, Rb (Vicencio et al. 2008; Childs et al. 2014), p21 (Zhang et al. 2005; Hsu et al. 2019), and p16 (Panmeer Selvam et al. 2018), that govern the choice between senescence, apoptosis, and repair and proliferation, depending on cell type (Vicencio et al. 2008) and the amount of damage or stress incurred (Childs et al. 2014).

As a corollary of these conclusions from expression profiling, we note that cell cycle and DNA repair genes, classically known to be repressed during senescence (Kim, Byun, et al. 2013; Chan et al. 2022), did not hit a floor of expression in senescent cultures: we could detect them at even lower expression levels upon *Usf2* knockdown. Since our cultures comprise >99% arrested cells within several days of irradiation (see Methods), the emerging picture is that the proliferation machinery is maintained at non-zero levels even in such a population. Any ability of these gene products to regain activity could be of particular interest as a potential mediator of the return to proliferation seen among senescent cells in certain scenarios (Beauséjour et al. 2003; Lee and Schmitt 2019).

Our work leaves open the mechanisms by which USF2 exerts its effects in the DNA damage response and cellular senescence. It is tempting to speculate that USF2 ultimately works in these processes in concert with its better-studied family member, USF1. Indeed, USF1 has been implicated in DNA repair (Baron et al. 2012), inflammation (Ruuth et al. 2018; Song et al. 2018), immune responses (Corre and Galibert 2005), and p53-mediated cell cycle arrest (Bouafia et al. 2014) in contexts other than senescence. In addition, given that USF2 has been implicated in the TGF $\beta$ -p53 axis in apoptosis (Sato et al. 2011) and fibrosis (Samarakoon et al. 2012), the latter pathway could mediate some part of the USF2 effects we have seen. Furthermore, regulatory network reconstruction (Roy et al. 2013) suggests that USF2 acts upstream of several

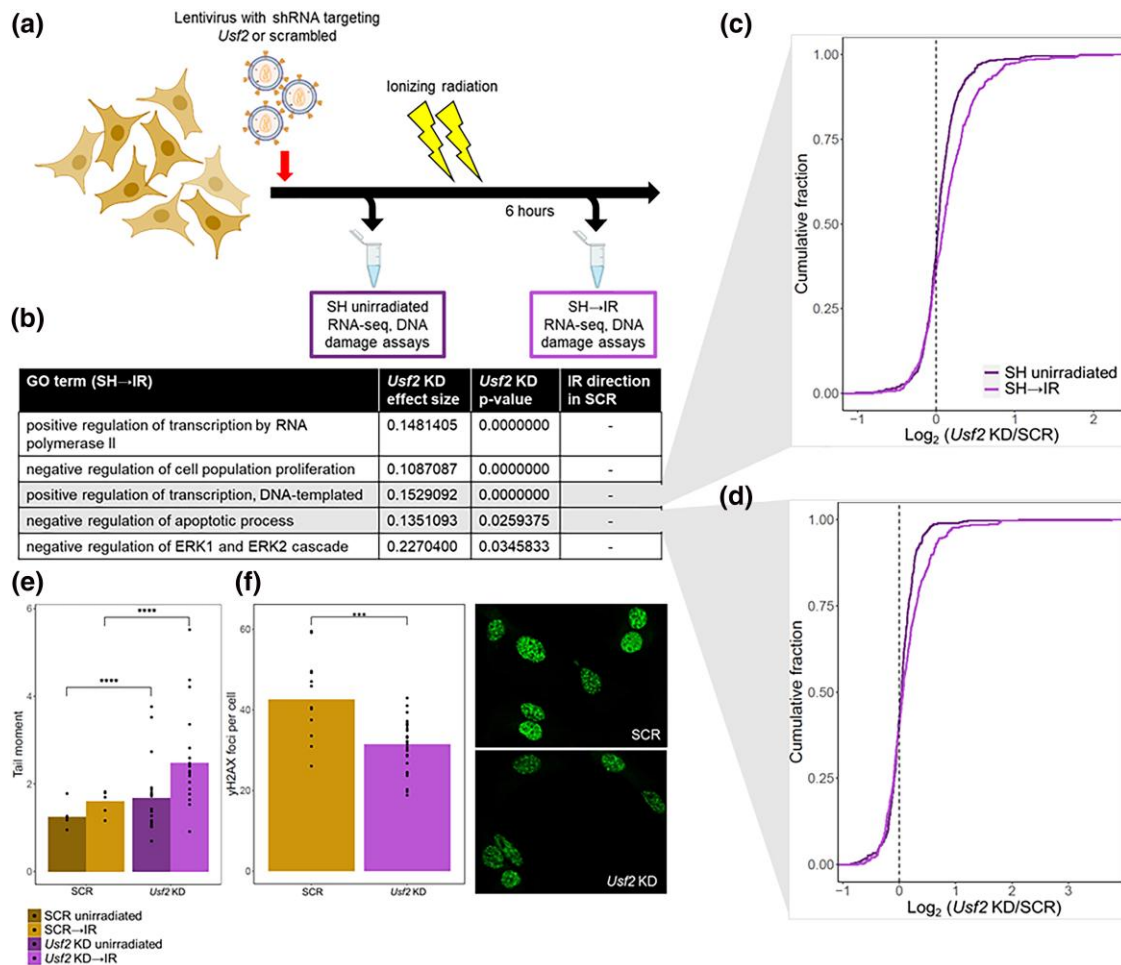


**Fig. 5.** *Usf2* depletion results in more DNA damage but a muted DNA damage response following irradiation. a) *M. musculus* primary fibroblasts were infected with a lentivirus encoding a short hairpin RNA (shRNA, SH) targeting *Usf2* or a scrambled control (SCR), and analyzed before (SH unirradiated) or 6 hours after (SH→IR) treatment with ionizing radiation. b) In a given row, the second column reports the average, across genes of the indicated Gene Ontology term, of the  $\log_2$  of the ratio of expression between *Usf2* knockdown (KD) and SCR-treated cells, 6 hours after irradiation. The third column reports significance in a resampling-based test for enrichment of directional differential expression between *Usf2* KD and SCR-treated cells in the respective term, corrected for multiple testing. The fourth column reports the direction of the change in expression 6 hours after irradiation in SCR-treated cells. c) Each trace reports a cumulative distribution of the  $\log_2$  of the ratio of expression between *Usf2* KD or SCR-treated cells in genes annotated in the positive regulation of transcription, before or 6 hours after irradiation treatment. The y-axis reports the proportion of genes with the expression change on the x-axis. d) Data are as in (C), except that genes involved in apoptosis were analyzed. e) Each column reports tail moments detected in a comet assay on primary fibroblasts harboring the indicated shRNAs, before or 6 hours after irradiation. In a given column, points report biological and technical replicates, and the bar height reports their average (SCR  $n = 5$ , *Usf2* KD  $n = 20$ ). \*\*\*\*,  $P < 0.0001$ , one-tailed Wilcoxon test. f) Left, each column reports number of  $\gamma$ H2AX foci per cell detected in primary fibroblasts harboring the indicated shRNAs 6 hours after irradiation. Data are displayed as in (e) (SCR  $n = 12$ , *Usf2* KD  $n = 28$ ). \*\*\*,  $P < 0.001$ , one-tailed Wilcoxon test. Right, representative images of the indicated cultures.

other transcription factors (KLF3, GLI3, and NFIL3) with direct targets in DNA repair, DNA damage response, and senescence pathways (Supplementary Table 11).

Alongside our use of cis-regulatory variation between mouse species as a screening tool for senescence genes, we also characterized overall patterns of divergence between *M. spretus* senescent cells and those of *M. musculus*. Given that the former exhibited lower levels of SASP mRNAs and proteins, we suggest that the rheostat of the senescence response is at a higher set point in this species, such that at a given level of stress (e.g. the irradiation we study here), cells of this species synthesize and secrete less of the SASP. Under this model, the decision set point for commitment to senescence by irradiated cells is similar across species, and, considered at any given time after damage exposure, it is the amplitude of the SASP that has been tuned by evolution. Such an idea would have precedent in the gradual ramp-up of senescence expression in *M. musculus* cells (Chan et al. 2022);

plausibly, *M. spretus* could be hard-wired for slower kinetics of this progression, in the fibroblasts we study here. *M. spretus* cells could also simply cap the amplitude of their SASP, limiting the immune recruitment function of senescent cells at any timepoint.

We further hypothesize that the dampened SASP might be a proximal cause for the lower SABG activity we have seen in *M. spretus* cells. Such a link would follow from current models of the senescent state in which production and secretion of SASP components (Dörr et al. 2013) lead to proteotoxic stress from insoluble aggregates (Brunk and Terman 2002; Park et al. 2018), an increase in the number and size of lysosomes (Kurz et al. 2000), and enhanced  $\beta$ -galactosidase activity (Lee et al. 2006). Plausibly, any of the phenotypes we study here in cell culture could have consequences in vivo, with potential links to the stress- and pathogen-resistance phenotypes characterized in *M. spretus* (Vanlaere et al. 2008; Dejager et al. 2009; Blanchet et al. 2011; Pérez del Villar et al. 2013; Pinheiro et al. 2013).

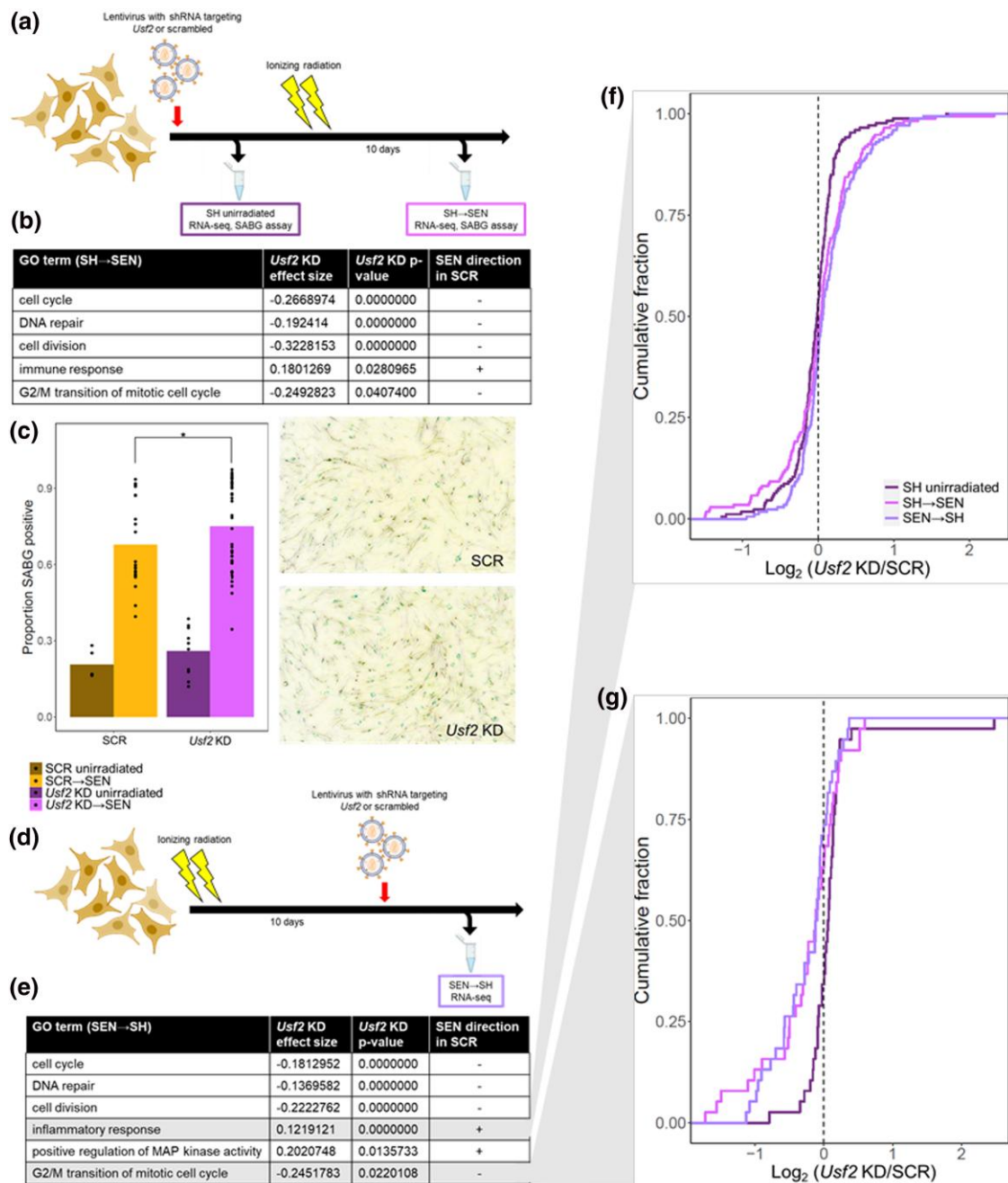


**Fig. 6.** *Usf2* knockdown results in an enhanced senescence profile. a) *M. musculus* primary fibroblasts were infected with a lentivirus encoding an shRNA (SH) targeting *Usf2* or a scrambled control, and analyzed before (SH unirradiated) or after (SH→SEN) treatment with ionizing radiation (IR) to induce senescence (SEN). b) Data are as in Fig. 5b except that cells were analyzed 10 days after irradiation. c) Left, each column reports the proportion of SABG-positive cells treated with the indicated shRNAs in resting culture (unirradiated) or 7 days after irradiation (SEN) as in (a). In a given column, points report biological and technical replicates, and the bar height reports their average (SCR unirradiated  $n = 5$ , SCR SEN  $n = 21$ , *Usf2* KD unirradiated  $n = 10$ , *Usf2* KD SEN  $n = 42$ ). \*,  $P < 0.05$ , one-tailed Wilcoxon test. Right, representative images of the indicated cultures. d) *M. musculus* primary fibroblasts were irradiated, incubated for 10 days to senesce, then infected with shRNAs, and analyzed after 10 additional days. e) Each trace reports a cumulative distribution of the  $\log_2$  of the ratio of expression in *Usf2* knockdown (KD) and scrambled control (SCR)-treated cells, in genes annotated in the inflammatory response, when shRNAs were administered to a resting culture (SH unirradiated), to resting cells followed by irradiation as in (a) (SH→SEN), or after irradiation and senescence establishment as in (c) (SEN→SH). The y-axis reports the proportion of genes with the expression change on the x-axis, with the latter taken as an average across replicates. f) Data are as in (e), except that genes involved in G2/M transition of mitotic cell cycle were analyzed.

The low-amplitude senescence program we have seen in *M. spretus* provides an intriguing contrast to the trend for fibroblasts from naked mole rat in culture to avoid both senescence and apoptosis altogether, after irradiation (Zhao et al. 2018). Instead, a given naked mole rat cell can often resolve DNA damage sufficiently to re-enter the cell cycle, to a degree several-fold

beyond that seen in *M. musculus*. Likewise, the beaver allele of the DNA damage factor SIRT6 confers a similar effect in a heterologous system (Tian et al. 2019). These represent evolutionary innovations in other rodents distinct from the quantitative tuning of senescence expression we have traced in *Mus*. The emerging picture is one in which no single irradiation response mechanism

manifests in all species, even in the simplest cell culture systems. Indeed, against the backdrop of the classic literature on *M. musculus* senescence (Itahana *et al.* 2004; Coppé, Patil, *et al.* 2010), many other irradiation response behaviors may remain to be discovered in additional non-model species. Human cells exhibit an avid senescence response, on par with that of *M. musculus* (Coppé, Patil, *et al.* 2010). As such, the programs nature has invented in other lineages may hold promise in the search for therapeutics that would tamp down the pro-aging effects of senescence in a clinical context.

## Data availability

Expression datasets supporting the conclusions of this article are available in the NCBI Gene Expression Omnibus (GEO; <https://www.ncbi.nlm.nih.gov/geo/>) under accession number GSE201217. Raw data and complete MS datasets have been uploaded to the Mass Spectrometry Interactive Virtual Environment repository, developed by the Center for Computational Mass Spectrometry at the University of California San Diego (MassIVE ID number: MSV000089246; ProteomeXchange ID: PXD033182).

[Supplemental material](#) available at G3 online.

## Acknowledgements

The authors thank Mary West for support of cell culture resources, Melissa Chao for help with data collection, Michael Nachman for *M. domesticus* animal material, and Herbert Kasler, Marius Walter, and Eric Verdin for helpful discussions and materials.

## Funding

This work was supported by National Institutes of Health R01 NS116992 and R01 GM120430 to RBB and R01 HD094787 to JMG. EEKK was supported by the National Science Foundation Graduate Research Fellowship Program (DGE-1313190). Any opinions, findings, and conclusions or recommendations expressed in this material are those of the author(s) and do not necessarily reflect the views of the National Science Foundation or the National Institutes of Health.

## Conflicts of interest statement

The author(s) declare no conflict of interest.

## Author contributions

RBB and TK conceived of the idea of the study; TK carried out fibroblast harvest and culture, RNA-seq, knockdown, and cell-biological assays and all data analysis. B.S. and C.D.K. carried out proteomics profiling. ECKK, ECM, and JMG carried out all mouse mating and husbandry. TK, JC, and RBB wrote the manuscript with input from all authors.

## Ethics declarations

*Ethics approval and consent to participate:* All methods used in animal husbandry and sample collection were approved under Montana Institutional Animal Care and Use Committee protocol number 062-1JGDBS-120418 and UC Berkeley Institutional Animal Care and Use Committee protocol number AUP-2016-03-8548-2, and reported in accordance with the ARRIVE guidelines ([\[arriveguidelines.org\]\(https://arriveguidelines.org\)\). All other methods described were performed in accordance with the rules and regulations of the corresponding institutions.](https://</a></p>
</div>
<div data-bbox=)

*Consent for publication:* Not applicable.

## Literature cited

- Allen RR, Qi L, Higgins PJ. Upstream stimulatory factor regulates E box-dependent PAI-1 transcription in human epidermal keratinocytes. *J Cell Physiol.* 2005;203(1):156–165. doi:10.1002/jcp.20211.
- Aperlo C, Boulukos KE, Pognonec P. The basic region/helix-loop-helix/leucine repeat transcription factor USF interferes with Ras transformation. *Eur J Biochem.* 1996;241(1):249–253. doi:10.1111/j.1432-1033.1996.0249t.x.
- Ashburner M, Ball CA, Blake JA, Botstein D, Butler H, Cherry JM, Davis AP, Dolinski K, Dwight SS, Eppig JT, *et al.* Gene Ontology: tool for the unification of biology. *Nat Genet.* 2000;25(1):25–29. doi:10.1038/75556.
- Baker DJ, Wijshake T, Tchkonja T, LeBrasseur NK, Childs BG, van de Sluis B, Kirkland JL, van Deursen JM. Clearance of p16Ink4a-positive senescent cells delays ageing-associated disorders. *Nature.* 2011;479(7372):232–236. doi:10.1038/nature10600.
- Bakkenist CJ, Drissi R, Wu J, Kastan MB, Dome JS. Disappearance of the telomere dysfunction-induced stress response in fully senescent cells. *Cancer Res.* 2004;64(11):3748–3752. doi:10.1158/0008-5472.CAN-04-0453.
- Bandyopadhyay D, Okan NA, Bales E, Nascimento L, Cole PA, Medrano EE. Down-regulation of p300/CBP histone acetyltransferase activates a senescence checkpoint in human melanocytes. *Cancer Res.* 2002;62(21):6231–6239.
- Baron Y, Corre S, Mouchet N, Vaulont S, Prince S, Galibert M-D. USF-1 Is critical for maintaining genome integrity in response to UV-induced DNA photolesions. *PLoS Genet.* 2012;8(1):e1002470. doi:10.1371/journal.pgen.1002470.
- Basisty N, Kale A, Jeon OH, Kuehnemann C, Payne T, Rao C, Holtz A, Shah S, Sharma V, Ferrucci L, *et al.* A proteomic atlas of senescence-associated secretomes for aging biomarker development. *PLoS Biol.* 2020;18(1):e3000599. doi:10.1371/journal.pbio.3000599.
- Beauséjour CM, Krtolica A, Galimi F, Narita M, Lowe SW, Yaswen P, Campisi J. Reversal of human cellular senescence: roles of the p53 and p16 pathways. *EMBO J.* 2003;22(16):4212–4222. doi:10.1093/emboj/cdg417.
- Blanchet C, Jaubert J, Carniel E, Fayolle C, Milon G, Szatanik M, Panthier J-J, Montagutelli X. Mus spretus SEG/Pas mice resist virulent *Yersinia pestis*, under multigenic control. *Genes Immun.* 2011;12(1):23–30. doi:10.1038/gene.2010.45.
- Bouafia A, Corre S, Gilot D, Mouchet N, Prince S, Galibert M-D. P53 requires the stress sensor USF1 to direct appropriate cell fate decision. *PLoS Genet.* 2014;10(5):e1004309. doi:10.1371/journal.pgen.1004309.
- Brückmann NH, Bennesen SN, Duijff PHG, Terp MG, Thomassen M, Larsen M, Pedersen CB, Kruse T, Alcaraz N, Ditzel HJ, *et al.* A functional genetic screen identifies the Mediator complex as essential for SSX2-induced senescence. *Cell Death Dis.* 2019;10(11):841. doi:10.1038/s41419-019-2068-1.
- Brunk UT, Terman A. Lipofuscin: mechanisms of age-related accumulation and influence on cell function. *Free Radic Biol Med.* 2002;33(5):611–619. doi:10.1016/s0891-5849(02)00959-0.
- Campisi J. Senescent cells, tumor suppression, and organismal aging: good citizens, bad neighbors. *Cell.* 2005;120(4):513–522. doi:10.1016/j.cell.2005.02.003.

- Campisi J. Aging, cellular senescence, and cancer. *Annu Rev Physiol.* 2013;75:685–705. doi:10.1146/annurev-physiol-030212-183653.
- Campisi J, d'Adda di Fagagna F. Cellular senescence: when bad things happen to good cells. *Nat Rev Mol Cell Biol.* 2007;8(9):729–740. doi:10.1038/nrm2233.
- Casella G, Munk R, Kim KM, Piao Y, De S, Abdelmohsen K, Gorospe M. Transcriptome signature of cellular senescence. *Nucleic Acids Res.* 2019;47(14):7294–7305. doi:10.1093/nar/gkz555.
- Chen J-H, Ozanne SE. Deep senescent human fibroblasts show diminished DNA damage foci but retain checkpoint capacity to oxidative stress. *FEBS Lett.* 2006;580(28–29):6669–6673. doi:10.1016/j.febslet.2006.11.023.
- Chen N, Szentirmay MN, Pawar SA, Sirito M, Wang J, Wang Z, Zhai Q, Yang H-X, Peehl DM, Ware JL, et al. Tumor-suppression function of transcription factor USF2 in prostate carcinogenesis. *Oncogene.* 2006;25(4):579–587. doi:10.1038/sj.onc.1209079.
- Chan M, Yuan H, Soifer I, Maile TM, Wang RY, Ireland A, O'Brien JJ, Goudeau J, Chan LJ, Vijay T, et al. 2022. Novel insights from a multiomics dissection of the Hayflick limit. *eLife.* 11:e70283. doi:10.7554/eLife.70283.
- Chi TF, Khoder-Agha F, Mennerich D, Kellokumpu S, Miinalainen I, Kietzmann T, Dimova EY. Loss of USF2 promotes proliferation, migration and mitophagy in a redox-dependent manner. *Redox Biol.* 2020;37:101750. doi:10.1016/j.redox.2020.101750.
- Childs BG, Baker DJ, Kirkland JL, Campisi J, van Deursen JM. Senescence and apoptosis: dueling or complementary cell fates? *EMBO Rep.* 2014;15(11):1139–1153. doi:10.15252/embr.201439245.
- Coppé J-P, Desprez P-Y, Krtolica A, Campisi J. The senescence-associated secretory phenotype: the dark side of tumor suppression. *Annu Rev Pathol.* 2010;5:99–118. doi:10.1146/annurev-pathol-121808-102144.
- Coppé J-P, Patil CK, Rodier F, Krtolica A, Beauséjour CM, Parrinello S, Hodgson JG, Chin K, Desprez P-Y, Campisi J. A human-like senescence-associated secretory phenotype is conserved in mouse cells dependent on physiological oxygen. *PLoS One.* 2010;5(2):e9188. doi:10.1371/journal.pone.0009188.
- Coppé J-P, Patil CK, Rodier F, Sun Y, Muñoz DP, Goldstein J, Nelson PS, Desprez P-Y, Campisi J. Senescence-associated secretory phenotypes reveal cell-nonautonomous functions of oncogenic RAS and the p53 tumor suppressor. *PLoS Biol.* 2008;6(12):2853–2868. doi:10.1371/journal.pbio.0060301.
- Corre S, Galibert M-D. Upstream stimulating factors: highly versatile stress-responsive transcription factors. *Pigment Cell Res.* 2005;18(5):337–348. doi:10.1111/j.1600-0749.2005.00262.x.
- Danecek P, Bonfield JK, Liddle J, Marshall J, Ohan V, Pollard MO, Whitwham A, Keane T, McCarthy SA, Davies RM, et al. Twelve years of SAMtools and BCFtools. *GigaScience.* 2021;10(2):giab008. doi:10.1093/gigascience/giab008.
- Davalos AR, Coppe J-P, Campisi J, Desprez P-Y. Senescent cells as a source of inflammatory factors for tumor progression. *Cancer Metastasis Rev.* 2010;29(2):273–283. doi:10.1007/s10555-010-9220-9.
- Dejager L, Libert C, Montagutelli X. Thirty years of *Mus spretus*: a promising future. *Trends Genet.* 2009;25(5):234–241. doi:10.1016/j.tig.2009.03.007.
- Demaria M, Ohtani N, Youssef SA, Rodier F, Toussaint W, Mitchell JR, Laberge R-M, Vijg J, Van Steeg H, Dollé MET, et al. An essential role for senescent cells in optimal wound healing through secretion of PDGF-AA. *Dev Cell.* 2014;31(6):722–733. doi:10.1016/j.devcel.2014.11.012.
- Dimri GP, Lee X, Basile G, Acosta M, Scott G, Roskelley C, Medrano EE, Linskens M, Rubelj I, Pereira-Smith O. A biomarker that identifies senescent human cells in culture and in aging skin in vivo. *Proc Natl Acad Sci U S A.* 1995;92(20):9363–9367. doi:10.1073/pnas.92.20.9363.
- Dörr JR, Yu Y, Milanovic M, Beuster G, Zasada C, Däbritz JHM, Lisec J, Lenze D, Gerhardt A, Schleicher K, et al. Synthetic lethal metabolic targeting of cellular senescence in cancer therapy. *Nature.* 2013;501(7467):421–425. doi:10.1038/nature12437.
- Fumagalli M, Rossiello F, Mondello C, d'Adda di Fagagna F. Stable cellular senescence is associated with persistent DDR activation. *PLoS One.* 2014;9(10):e110969. doi:10.1371/journal.pone.0110969.
- Gene Ontology Consortium. The Gene Ontology resource: enriching a GOLD mine. *Nucleic Acids Res.* 2021;49(D1):D325–D334. doi:10.1093/nar/gkaa1113.
- Han R, Li L, Ugalde AP, Tal A, Manber Z, Barbera EP, Chiara VD, Elkon R, Agami R. Functional CRISPR screen identifies AP1-associated enhancer regulating FOXF1 to modulate oncogene-induced senescence. *Genome Biol.* 2018;19(1):118. doi:10.1186/s13059-018-1494-1.
- Hayflick L. The limited in vitro lifetime of human diploid cell strains. *Exp Cell Res.* 1965;37(3):614–636. doi:10.1016/0014-4827(65)90211-9.
- Heinz S, Romanoski CE, Benner C, Allison KA, Kaikkonen MU, Orozco LD, Glass CK. Effect of natural genetic variation on enhancer selection and function. *Nature.* 2013;503(7477):487–492. doi:10.1038/nature12615.
- Hsu C-H, Altschuler SJ, Wu LF. Patterns of early p21 dynamics determine proliferation-senescence cell fate after chemotherapy. *Cell.* 2019;178(2):361–373.e12. doi:10.1016/j.cell.2019.05.041.
- Hu D, Tjon EC, Andersson KM, Molica GM, Pham MC, Healy B, Murugaiyan G, Pochet N, Kuchroo VK, Bokarewa MI, et al. Aberrant expression of USF2 in refractory rheumatoid arthritis and its regulation of proinflammatory cytokines in Th17 cells. *Proc Natl Acad Sci U S A.* 2020;117(48):30639–30648. doi:10.1073/pnas.2007935117.
- Huang R-X, Zhou P-K. DNA Damage response signaling pathways and targets for radiotherapy sensitization in cancer. *Signal Transduct Target Ther.* 2020;5(1):60. doi:10.1038/s41392-020-0150-x.
- Itahana K, Campisi J, Dimri GP. Mechanisms of cellular senescence in human and mouse cells. *Biogerontology.* 2004;5(1):1–10. doi:10.1023/b:bgen.0000017682.96395.10.
- Kale A, Sharma A, Stolzing A, Desprez P-Y, Campisi J. Role of immune cells in the removal of deleterious senescent cells. *Immun Ageing.* 2020;17(1):16. doi:10.1186/s12979-020-00187-9.
- Kang C. Senolytics and senostatics: a two-pronged approach to target cellular senescence for delaying aging and age-related diseases. *Mol Cells.* 2019;42(12):821–827. doi:10.14348/molcells.2019.0298.
- Khan M, Gasser S. Generating primary fibroblast cultures from mouse ear and tail tissues. *J Vis Exp.* 2016;(107):53565. doi:10.3791/53565.
- Kim Y-M, Byun H-O, Jee BA, Cho H, Seo Y-H, Kim Y-S, Park MH, Chung H-Y, Woo HG, Yoon G. Implications of time-series gene expression profiles of replicative senescence. *Aging Cell.* 2013;12(4):622–634. doi:10.1111/acer.12087.
- Kim E-C, Kim J-R. Senotherapeutics: emerging strategy for healthy aging and age-related disease. *BMB Rep.* 2019;52(1):47–55. doi:10.5483/BMBRep.2019.52.1.293.
- Kim EK, Moon S, Kim DK, Zhang X, Kim J. CXCL1 Induces senescence of cancer-associated fibroblasts via autocrine loops in oral squamous cell carcinoma. *PLoS One.* 2018;13(1):e0188847. doi:10.1371/journal.pone.0188847.
- Kim D, Pertea G, Trapnell C, Pimentel H, Kelley R, Salzberg SL. TopHat2: accurate alignment of transcriptomes in the presence

- of insertions, deletions and gene fusions. *Genome Biol.* 2013; 14(4):R36. doi:10.1186/gb-2013-14-4-r36.
- Krtolica A, Parrinello S, Lockett S, Desprez PY, Campisi J. Senescent fibroblasts promote epithelial cell growth and tumorigenesis: a link between cancer and aging. *Proc Natl Acad Sci U S A.* 2001;98(21):12072–12077. doi:10.1073/pnas.211053698.
- Kurz DJ, Decary S, Hong Y, Erusalimsky JD. Senescence-associated (beta)-galactosidase reflects an increase in lysosomal mass during replicative ageing of human endothelial cells. *J Cell Sci.* 2000;113(Pt 20):3613–3622. doi:10.1242/jcs.113.20.3613.
- Langmead B, Salzberg SL. Fast gapped-read alignment with Bowtie 2. *Nat Methods.* 2012;9(4):357–359. doi:10.1038/nmeth.1923.
- Lee BY, Han JA, Im JS, Morrone A, Johung K, Goodwin EC, Kleijer WJ, DiMaio D, Hwang ES. Senescence-associated beta-galactosidase is lysosomal beta-galactosidase. *Aging Cell.* 2006;5(2):187–195. doi:10.1111/j.1474-9726.2006.00199.x.
- Lee S, Schmitt CA. The dynamic nature of senescence in cancer. *Nat Cell Biol.* 2019;21(1):94–101. doi:10.1038/s41556-018-0249-2.
- Levi N, Papisov N, Solomonov I, Sagi I, Krizhanovsky V. The ECM path of senescence in aging: components and modifiers. *FEBS J.* 2020;287(13):2636–2646. doi:10.1111/febs.15282.
- Li H. A statistical framework for SNP calling, mutation discovery, association mapping and population genetic parameter estimation from sequencing data. *Bioinforma.* 2011;27(21):2987–2993. doi:10.1093/bioinformatics/btr509.
- Li H, Handsaker B, Wysoker A, Fennell T, Ruan J, Homer N, Marth G, Abecasis G, Durbin R; 1000 Genome Project Data Processing Subgroup. The sequence alignment/map format and SAMtools. *Bioinforma.* 2009;25(16):2078–2079. doi:10.1093/bioinformatics/btp352.
- Livak KJ, Schmittgen TD. Analysis of relative gene expression data using real-time quantitative PCR and the 2- $\Delta\Delta$ CT method. *Methods.* 2001;25(4):402–408. doi:10.1006/meth.2001.1262.
- Martínez-Zamudio RI, Roux P-F, de Freitas JANLF, Robinson L, Doré G, Sun B, Belenki D, Milanovic M, Herbig U, Schmitt CA, et al. AP-1 imprints a reversible transcriptional programme of senescent cells. *Nat Cell Biol.* 2020;22(7):842–855. doi:10.1038/s41556-020-0529-5.
- Neri F, Basisty N, Desprez P-Y, Campisi J, Schilling B. Quantitative proteomic analysis of the senescence-associated secretory phenotype by data-independent acquisition. *Curr Protoc.* 2021; 1(2):e32. doi:10.1002/cpz1.32.
- Nickoloff JA, Boss M-K, Allen CP, LaRue SM. Translational research in radiation-induced DNA damage signaling and repair. *Transl Cancer Res.* 2017;6(Suppl 5):S875–S891. doi:10.21037/tcr.2017.06.02.
- Olive PL, Banáth JP. The comet assay: a method to measure DNA damage in individual cells. *Nat Protoc.* 2006;1(1):23–29. doi:10.1038/nprot.2006.5.
- Olivieri F, Prattichizzo F, Grillari J, Balistreri CR. Cellular senescence and inflammaging in age-related diseases. *Mediators Inflamm.* 2018;2018:9076485. doi:10.1155/2018/9076485.
- Panneer Selvam S, Roth BM, Nganga R, Kim J, Cooley MA, Helke K, Smith CD, Ogretmen B. Balance between senescence and apoptosis is regulated by telomere damage-induced association between p16 and caspase-3. *J Biol Chem.* 2018;293(25):9784–9800. doi:10.1074/jbc.RA118.003506.
- Paramos-de-Carvalho D, Jacinto A, Saúde L. The right time for senescence. *Elife.* 2021;10:e72449. doi:10.7554/eLife.72449.
- Park JT, Lee Y-S, Cho KA, Park SC. Adjustment of the lysosomal-mitochondrial axis for control of cellular senescence. *Ageing Res Rev.* 2018;47:176–182. doi:10.1016/j.arr.2018.08.003.
- Parrinello S, Coppe J-P, Krtolica A, Campisi J. Stromal-epithelial interactions in aging and cancer: senescent fibroblasts alter epithelial cell differentiation. *J Cell Sci.* 2005;118(Pt 3):485–496. doi:10.1242/jcs.01635.
- Pawar SA, Szentirmay MN, Hermeking H, Sawadogo M. Evidence for a cancer-specific switch at the CDK4 promoter with loss of control by both USF and c-Myc. *Oncogene.* 2004;23(36):6125–6135. doi:10.1038/sj.onc.1207806.
- Pérez del Villar L, Vicente B, Galindo-Villardón P, Castellanos A, Pérez-Losada J, Muro A. *Schistosoma mansoni* experimental infection in *Mus spretus* (SPRET/Eij strain) mice. *Parasite.* 2013;20: 27. doi:10.1051/parasite/2013027.
- Pinhoiro I, Dejager L, Petta I, Vandevyver S, Puimège L, Mahieu T, Ballegeer M, Van Hauwermeiren F, Riccardi C, Vuylsteke M, et al. LPS Resistance of SPRET/Ei mice is mediated by Gilz, encoded by the Tsc22d3 gene on the X chromosome. *EMBO Mol Med.* 2013; 5(3):456–470. doi:10.1002/emmm.201201683.
- Pluquet O, Pourtier A, Abbadie C. The unfolded protein response and cellular senescence. A review in the theme: cellular mechanisms of endoplasmic reticulum stress signaling in health and disease. *Am J Physiol Cell Physiol.* 2015;308(6):C415–C425. doi:10.1152/ajpcell.00334.2014.
- Podhorecka M, Skladanowski A, Bozko P. H2AX phosphorylation: its role in DNA damage response and cancer therapy. *J Nucleic Acids.* 2010;2010:920161. doi:10.4061/2010/920161.
- Purcell M, Kruger A, Tainsky MA. Gene expression profiling of replicative and induced senescence. *Cell Cycle.* 2014;13(24): 3927–3937. doi:10.4161/15384101.2014.973327.
- Putri GH, Anders S, Pyl PT, Pimanda JE, Zanini F. Analysing high-throughput sequencing data in Python with HTSeq 2.0. *Bioinformatics.* 2022;38(10):2943–2945. doi:10.1093/bioinformatics/btac166.
- Qi L, Allen RR, Lu Q, Higgins CE, Garone R, Staiano-Coico L, Higgins PJ. PAI-1 transcriptional regulation during the G0 → G1 transition in human epidermal keratinocytes. *J Cell Biochem.* 2006;99(2): 495–507. doi:10.1002/jcb.20885.
- Qi L, Higgins CE, Higgins SP, Law BK, Simone TM, Higgins PJ. The basic helix-loop-helix/leucine zipper transcription factor USF2 integrates serum-induced PAI-1 expression and keratinocyte growth. *J Cell Biochem.* 2014;115(10):1840–1847. doi:10.1002/jcb.24861.
- Qyang Y, Luo X, Lu T, Ismail PM, Krylov D, Vinson C, Sawadogo M. Cell-type-dependent activity of the ubiquitous transcription factor USF in cellular proliferation and transcriptional activation. *Mol Cell Biol.* 1999;19(2):1508–1517. doi:10.1128/MCB.19.2.1508.
- Redon CE, Dickey JS, Bonner WM, Sedelnikova OA.  $\gamma$ -H2AX as a biomarker of DNA damage induced by ionizing radiation in human peripheral blood lymphocytes and artificial skin. *Adv Space Res.* 2009;43(8):1171–1178. doi:10.1016/j.asr.2008.10.011.
- Rodier F, Coppé J-P, Patil CK, Hoeijmakers WAM, Muñoz DP, Raza SR, Freund A, Campeau E, Davalos AR, Campisi J. Persistent DNA damage signalling triggers senescence-associated inflammatory cytokine secretion. *Nat Cell Biol.* 2009;11(8):973–979. doi:10.1038/ncb1909.
- Roy S, Lagree S, Hou Z, Thomson JA, Stewart R, Gasch AP. Integrated module and gene-specific regulatory inference implicates upstream signaling networks. *PLoS Comput Biol.* 2013;9(10): e1003252. doi:10.1371/journal.pcbi.1003252.
- Ruuth M, Soronen J, Kaiharju E, Merikanto K, Perttilä J, Metso J, Lee-Rueckert M, Taskinen M-R, Kovanen PT, Öörni K, et al. USF1 Deficiency alleviates inflammation, enhances cholesterol efflux and prevents cholesterol accumulation in macrophages. *Lipids Health Dis.* 2018;17(1):285. doi:10.1186/s12944-018-0930-2.

- Salotti J, Johnson PF. Regulation of senescence and the SASP by the transcription factor C/EBP $\beta$ . *Exp Gerontol*. 2019;128:110752. doi:10.1016/j.exger.2019.110752.
- Samarakoon R, Overstreet JM, Higgins SP, Higgins PJ. TGF- $\beta$ 1  $\rightarrow$  SMAD/p53/USF2  $\rightarrow$  PAI-1 transcriptional axis in ureteral obstruction-induced renal fibrosis. *Cell Tissue Res*. 2012;347(1):117–128. doi:10.1007/s00441-011-1181-y.
- Santoro A, Spinelli CC, Martucciello S, Nori SL, Capunzo M, Puca AA, Ciaglia E. Innate immunity and cellular senescence: the good and the bad in the developmental and aged brain. *J Leukoc Biol*. 2018;103(3):509–524. doi:10.1002/JLB.3MR0118-003R.
- Sato AYS, Antonioli E, Tambellini R, Campos AH. ID1 Inhibits USF2 and blocks TGF- $\beta$ -induced apoptosis in mesangial cells. *Am J Physiol Renal Physiol*. 2011;301(6):F1260–F1269. doi:10.1152/ajprenal.00128.2011.
- Schneider CA, Rasband WS, Eliceiri KW. NIH Image to ImageJ: 25 years of image analysis. *Nat Methods*. 2012;9(7):671–675. doi:10.1038/nmeth.2089.
- Siddiqui MS, François M, Fenech MF, Leifert WR. Persistent  $\gamma$ H2AX: a promising molecular marker of DNA damage and aging. *Mutat Res Rev Mutat Res*. 2015;766:1–19. doi:10.1016/j.mrrev.2015.07.001.
- Silva E, Ideker T. Transcriptional responses to DNA damage. *DNA Repair (Amst)*. 2019;79:40–49. doi:10.1016/j.dnarep.2019.05.002.
- Song X, Zhu M, Hao L, Liu B, Yan Z, Wang W, Hongyi L, Sun J, Li S. USF1 Promotes the development of knee osteoarthritis by activating the NF- $\kappa$ B signaling pathway. *Exp Ther Med*. 2018;16(4):3518–3524. doi:10.3892/etm.2018.6608.
- Sun W, Hu Y. eQTL mapping using RNA-Seq data. *Stat Biosci*. 2013;5(1):198–219. doi:10.1007/s12561-012-9068-3.
- Tian X, Firsanov D, Zhihui Z, Cheng Y, Luo L, Tomblin G, Tan R, Simon M, Henderson S, Steffan J, et al. SIRT6 Is responsible for more efficient DNA double-strand break repair in long-lived Species. *Cell*. 2019;177(3):622–638.e22. doi:10.1016/j.cell.2019.03.043.
- Tyler EJ, Gutierrez Del Arroyo A, Hughes BK, Wallis R, Garbe JC, Stampfer MR, Koh J, Lowe R, Philpott MP, Bishop CL. Early growth response 2 (EGR2) is a novel regulator of the senescence programme. *Aging Cell*. 2021;20(3):e13318. doi:10.1111/acer.13318.
- Vanlaere I, Vanderrijst A, Guénet J-L, De Filette M, Libert C. Mx1 causes resistance against influenza A viruses in the *Mus spretus*-derived inbred mouse strain SPRET/Ei. *Cytokine*. 2008;42(1):62–70. doi:10.1016/j.cyto.2008.01.013.
- Venkata Narayanan I, Paulsen MT, Bedi K, Berg N, Ljungman EA, Francia S, Veloso A, Magnuson B, di Fagagna FD, Wilson TE, et al. Transcriptional and post-transcriptional regulation of the ionizing radiation response by ATM and p53. *Sci Rep*. 2017;7(1):43598. doi:10.1038/srep43598.
- Veyrieras J-B, Kudaravalli S, Kim SY, Dermitzakis ET, Gilad Y, Stephens M, Pritchard JK. High-resolution mapping of expression-QTLs yields insight into human gene regulation. *PLoS Genet*. 2008;4(10):e1000214. doi:10.1371/journal.pgen.1000214.
- Vicencio JM, Galluzzi L, Tajeddine N, Ortiz C, Criollo A, Tasdemir E, Morselli E, Ben Younes A, Maiuri MC, Lavandro S, et al. Senescence, apoptosis or autophagy? When a damaged cell must decide its path—a mini-review. *Gerontology*. 2008;54(2):92–99. doi:10.1159/000129697.
- Vierbuchen T, Ling E, Cowley CJ, Couch CH, Wang X, Harmin DA, Roberts CWM, Greenberg ME. AP-1 Transcription factors and the BAF Complex mediate signal-dependent enhancer selection. *Mol Cell*. 2017;68(6):1067–1082.e12. doi:10.1016/j.molcel.2017.11.026.
- Villarreal CA, Bastías M, Canessa P, Cubillos FA. Uncovering divergence in gene expression regulation in the adaptation of yeast to nitrogen scarcity. *mSystems*. 2021;6(4):e0046621. doi:10.1128/mSystems.00466-21.
- Wan M, Gray-Gaillard EF, Elisseeff JH. Cellular senescence in musculoskeletal homeostasis, diseases, and regeneration. *Bone Res*. 2021;9(1):1–12. doi:10.1038/s41413-021-00164-y.
- Wang Y, Sui Y, Lian A, Han X, Liu F, Zuo K, Liu M, Sun W, Wang Z, Liu Z, et al. PBX1 Attenuates hair follicle-derived mesenchymal stem cell senescence and apoptosis by alleviating reactive oxygen species-mediated DNA damage instead of enhancing DNA damage repair. *Front Cell Dev Biol*. 2021;9:739868. doi:10.3389/fcell.2021.739868.
- Wang Y, Xu Q, Sack L, Kang C, Elledge SJ. A gain-of-function senescence bypass screen identifies the homeobox transcription factor DLX2 as a regulator of ATM-p53 signaling. *Genes Dev*. 2016;30(3):293–306. doi:10.1101/gad.271445.115.
- Wittkopp PJ, Haerum BK, Clark AG. Evolutionary changes in cis and trans gene regulation. *Nature*. 2004;430(6995):85–88. doi:10.1038/nature02698.
- Xie Q, Peng S, Tao L, Ruan H, Yang Y, Li T-M, Adams U, Meng S, Bi X, Dong M-Q, et al. E2f transcription factor 1 regulates cellular and organismal senescence by inhibiting forkhead box O transcription factors. *J Biol Chem*. 2014;289(49):34205–34213. doi:10.1074/jbc.M114.587170.
- Yang MG, Ling E, Cowley CJ, Greenberg ME, Vierbuchen T. Characterization of sequence determinants of enhancer function using natural genetic variation. Parker SC, editor. *Elife*. 2022;11:e76500. doi:10.7554/eLife.76500.
- Yang K, Wang F, Zhang H, Wang X, Chen L, Su X, Wu X, Han Q, Chen Z, Chen Z-S, et al. Target inhibition of CBP induced cell senescence in BCR-ABL- T315I mutant chronic myeloid leukemia. *Front Oncol*. 2021;10:588641. doi:10.3389/fonc.2020.588641
- Yevshin I, Sharipov R, Kolmykov S, Kondrakhin Y, Kolpakov F. GTRD: a database on gene transcription regulation-2019 update. *Nucleic Acids Res*. 2019;47(D1):D100–D105. doi:10.1093/nar/gky1128.
- Zhang X, Li J, Sejas DP, Pang Q. The ATM/p53/p21 pathway influences cell fate decision between apoptosis and senescence in reoxygenated hematopoietic progenitor cells. *J Biol Chem*. 2005;280(20):19635–19640. doi:10.1074/jbc.M502262200.
- Zhang C, Zhang X, Huang L, Guan Y, Huang X, Tian X-L, Zhang L, Tao W. ATF3 Drives senescence by reconstructing accessible chromatin profiles. *Aging Cell*. 2021;20(3):e13315. doi:10.1111/acer.13315.
- Zhao H, Darzynkiewicz Z. Biomarkers of cell senescence assessed by imaging cytometry. *Methods Mol Biol*. 2013;965:83–92. doi:10.1007/978-1-62703-239-1\_5.
- Zhao Y, Tyshkovskiy A, Muñoz-Espín D, Tian X, Serrano M, de Magalhaes JP, Nevo E, Gladyshev VN, Seluanov A, Gorbunova V. Naked mole rats can undergo developmental, oncogene-induced and DNA damage-induced cellular senescence. *Proc Natl Acad Sci U S A*. 2018;115(8):1801–1806. doi:10.1073/pnas.1721160115.